Exploring QA methods for real-time MRI guided radiotherapy

Assessment of dose distributions on a 25ms timescale

H. Bergsma

TU Delft

Exploring QA methods for real-time MRI guided radiotherapy

by

H. Bergsma

to obtain the degree of Master of Science
At the Delft University of Technology

TU Delft

Student number:	1559850	
Project duration:	March, 2020 – March, 2021	
Thesis committee:	Prof. Dr. M. van Vulpen	TU Delft, supervisor
	Prof. Dr. B. Raaijmakers	UMC Utrecht, supervisor
	Dr. J. Wolthaus	UMC Utrecht, supervisor
	Dr. D. Lathouwers	TU Delft
	Prof. Dr. M.S. Hoogeman	TU Delft

An electronic version of this thesis is available at http://repository.tudelft.nl/

Abstract

Purpose:
The MR-linac is a novel hybrid system that is used in radiotherapy (RT) and combines irradiation with MR imaging. Novel adaptive image-guided radiotherapy techniques are developed for this machine. However, new quality assurance (QA) techniques are required that check if the (adapted) planned radiation dose is the same as the dose given to the patient. Dose reconstruction, based on the MR-LINACs logfile, can be a new powerful QA tool.
Here, we verify logfile based dose reconstruction with the treatment planning system (TPS) dose and Delta4 phantom MR+ on various timescale and discuss its potential as a new QA tool for the MR-LINAC.
Method:
Software was developed and validated for comparison of the different dose distributions. A patient RT-plan was selected with the intensity modulated RT step-and-shoot technique. The first experiment TPS dose – Logfile was performed at timescales: 1. Total RT-plan 2. Per beam. The second experiment Delta4 – Logfile was performed at timescales: 1. Total RT-plan 2. Per beam 3. Per segment 4. Per 200ms.
For analysis, visual comparison, dose profiles, dose difference (DD) and gamma-index (90% of the data) were used.
Results:
The patient RT-plan had 7 fields and 57 segments. Outcomes of the first experiment were: 1. Total RT-plan: DD = -1.5 to 1.5% and gamma-index (DD=1% & DTA=1mm) of 0.89. 2. Per beam: DD = -3.3 to 2.4% and gamma-index (DD=2% & DTA=2mm) of 0.87.
Outcomes of the second experiment were: 1. Total RT-plan: DD of -2.7 to 2.4% and a gamma-index (DD=2% and DTA=2mm) of 0.69. 2. Per beam: maximum DD of -4.7 to 2.5% and gamma-index (DD=2% and DTA=2mm) of 0.99 considering all beams. 3. Per segment: maximum DD of -5.9 to 6.0% and gamma-index (DD=3% and DTA=3mm) of 1.0 considering all segments. 4. Per 200ms: the cumulative DD in a high irradiated area was -4.0 to 7.1%, after the 2^{nd} segment and -5.2 to 5.3%,. after the 7^{th} segment.
Conclusion:
Logfile based dose reconstruction might be newest QA tool for the MR-LINAC. Accuracies meet current accepted criteria for IMRT treatment plans considering the total RT-plan and per beam timescale. Smaller timescales have a slightly higher error and require further optimization.

Table of contents

1. Introduction

In external beam radiotherapy (RT) high energy photon beams are used and aimed at an target (e.g. tumor). The goal of external beam RT is an accurate irradiation of the target with minimal damage to the surroundings (=organs at risk). An important aspect in the RT process is imaging of the patients anatomy. Prior to RT treatment, the patient is imaged with computed tomography (CT) or magnetic resonance imaging (MRI), a so called pre-treatment CT and/or MRI. These images are used as an input for the treatment planning system (TPS) to create a radiotherapy plan (RT plan). The treatment plan is a treatment prescription of field shapes, dose rates, gantry angles and other parameters. At treatment, the patient is first positioned and immobilized. Then, the linear accelerator (linac) irradiates the patient according to the treatment plan and finally, a post-delivery scan is acquired. In general, an RT treatment is split into multiple fractions of the total dose to reduce damage in organs at risk without compromising therapeutic outcome.

Between acquiring the planning CT/MRI and the start of RT treatment, as well as during RT, anatomical changes may take place. Ignoring these anatomical changes will result in a decline in target dose coverage [1], e.g. the tumor will not receive the intended dose. Therefore, up-to-date imaging is required before the start and possibly during RT treatment. In case of conventional RT (figure 2A), (integrated) Cone-beam Computed Tomography (CBCT) is used for the verification of patient set-up and tumor position [2], figure 2A step F. Nonetheless, CBCT has poor image quality with low tissue contrast. Therefore better imaging is desired for adaptation of the RT-plan.

Figure 1 – The Elekta Unity MR-LINAC situated in the University Medical Center (UMC) Utrecht.

1.1 Radiotherapy with the MR-LINAC

In the UMC Utrecht, patients are also treated on MR-linacs since 2017 (figure 1). An MR-linac is a hybrid 7 MV linac combined with a 1.5T MRI scanner that combines both irradiation and MR imaging into a single machine. One advantage of MR is that the images have superior soft tissue contrast, compared to (CB)CT [3]. Also custom optimization of the MR images is possible resulting in an enhancement of different tissue aspects. Moreover, MR is the currently the best diagnostic imaging modality for visualization of many tumors treated with radiotherapy [4].

1.2 MR-LINAC: Image guided radiotherapy

When the MR imaging capabilities are linked to the linac, image guidance of multiple sites throughout the body during treatment delivery becomes available. Here, the radiotherapy plan is adapted, based on the latest anatomy of the patient, so called image-guided adaptive radiotherapy (IgART).

Currently, daily adaptive MRI guided RT is used on the MR-linac (figure 2B). This method utilizes MR images which are acquired before and on the same day of the fractional RT. The new images are used for creating a new fractional RT plan (figure 2B, steps F-H) [5], [6]. Treatments with a daily new fractional RT plans can improve target coverage, for example in prostate cancer patients [7].

In the future, intrafractional adaptation will become possible on MR-LINAC systems. This form of RT uses up-to-date MR images, not only before the start, but also during the fractional RT treatments. This repeatedly results in new (adjusted) fractional RT plans. For example, movement caused by intrafractional organ motion are eliminated because of (real-time) feedback from the imaging system [8]. The patient can be irradiated as if no motion is present. The final results should lead to a better target coverage and lower irradiation of normal tissue (e.g. healthy organs). However, standard online plan verification is not possible, therefore alternative verification methods should be developed, which is the subject of quality assurance.

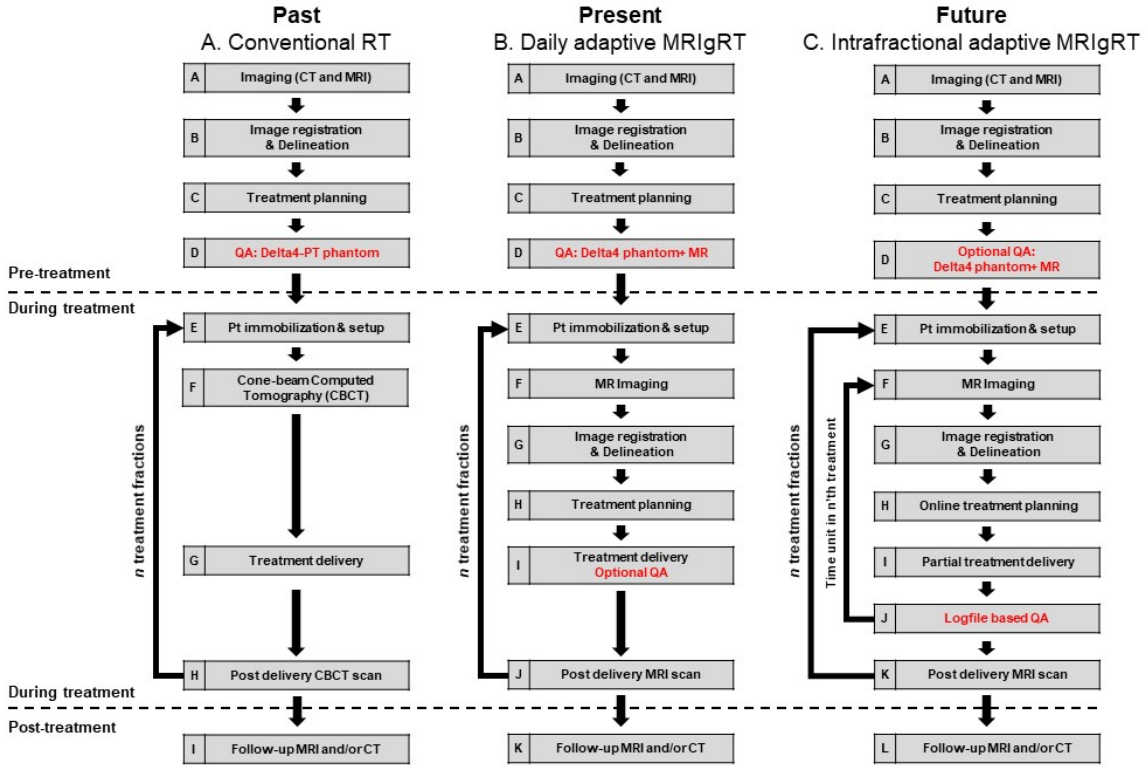

Figure 2 – Patient workflows for different forms of radiotherapy of the past (A), present (B) and future (C) including steps for Quality Assurance (QA), highlighted in red.

1.3 Quality Assurance (QA)

An important aspect of radiotherapy is quality assurance (QA), highlighted in red (figure 2). QA of treatment plans verifies that the delivered dose will be similar/equal to the planned dose. Several methods for plan QA are available, for example point measurements with an ionization chamber. This is an absolute dose method and verifies whether the recorded dose in the chamber is the expected dose in the volume. 2D dose measurements can be performed by using an array of ionization chambers or diodes, electronic portal imaging devices (EPIDs) and radio-chromic film [9]. These devices are often used for relative dose measurement. Frequently, an ionization chamber and a plane dose measurement device are combined, so that the relative plane dose measurements can be scaled to absolute doses. Three dimensional dose measurements can be performed by the Delta4 phantoms (Scandidos AB, Uppsala Sweden) which are diode array phantoms that have absolute dose outputs.

1.4 QA – Delta4 phantoms

The Delta4-PT phantom (Scandidos AB, Uppsala Sweden) is an cylindrical diode array phantom that contains 2 orthogonal boards with a total of 1069 detectors, see figure 3A. The detector planes subtend angles of 50° clockwise and 40° counter-clockwise with respect to the vertical axis. The role of the Delta4 PT phantom in conventional RT is patient QA of the dose distribution in the isocentric region. This results in the delivered dose of the target and organs at risk. The device is widely used in the clinic and its performance has been extensively investigated [10], [11].

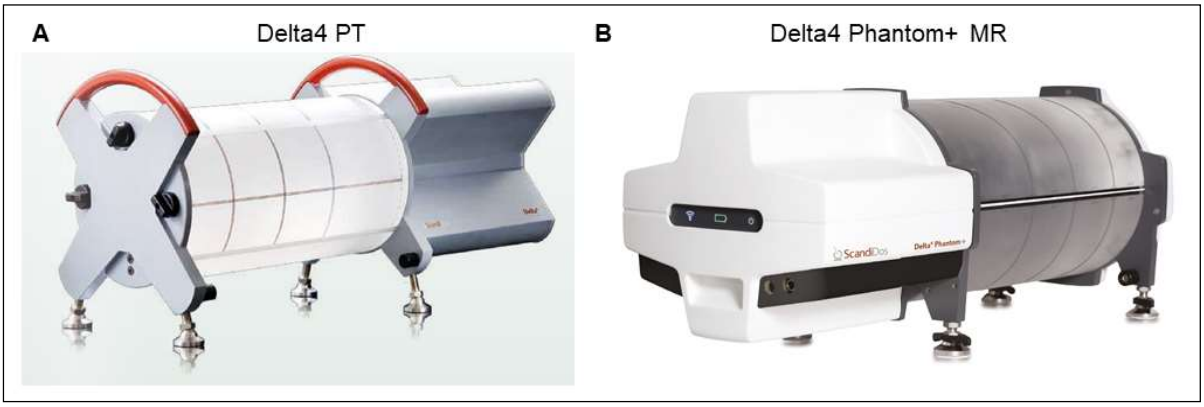

Figure 3 – Quality assurance with the Delta4-PT (A) used for conventional RT (figure 2A) and the Delta4 phantom+MR (B), used on the MR-LINAC for daily adaptive MR guided radiotherapy (figure 2B).

The Delta4 phantom+ MR is a modified Delta4-PT phantom . For use in the MR-LINAC, the feet of the device were taken off, adaptations were made to the network sockets and the power supply cables were extended for positioning of the power supply outside of the magnetic field area [12]. In this way no ferromagnetic objects where present which could cause heating, experience strong forces and/or cause artifacts [13]. The phantom consists of two crossing 2D arrays with a total of 1069 detectors and a fixed cylindrical geometry. Currently, the Delta4 phantom+ MR is used for plan QA on the MR-LINAC in the pre-treatment phase and optionally after a fractional treatment, see figure 2B (highlighted in red). When the RT treatment is finished, the Delta4 phantom is positioned and the RT-plan is executed for a second time. The measurements in combination with the initial planned dose result in the plan QA. This method is not suitable for future intrafractional adaptive MRIgRT (figure 2C). Logfile, generated by the MR-LINAC, may be an method for QA when using intrafractional adaptive MRIgRT.

1.5 Logfile based QA

Radiotherapy systems record actual axis information such as gantry/collimator angles, leafs, banks positions and monitor units (MUs) delivered. During the RT treatment, this information is stored into a log file and allows for comparison of the planned and the actual delivered data for each parameter. Logfiles can help give direction to the cause of a problem in case of troubleshooting. Moreover, it can also be used as an pre-treatment quality tool or as an instrument to ensure that the machine has correctly interpreted the RT plan [14].

The logfile combined with imaging can also be used to reconstruct the delivered radiotherapy dose. Several authors have demonstrated its potential for Volumetric-Modulated Arc Therapy (VMAT) using the patient's original CT [15] or the on-treatment cone-beam CT [16]. Also reonstruction of the delivered dose on the MR-LINAC have been performed [17], [18]. However, little has been published about logfile based dose reconstruction as a method for QA in intrafractional online MRIgRT.

1.6 Research questions and hypotheses

In this thesis we will explore logfile based dose reconstruction on the MR-LINAC at different dose time-intervals (time-resolved). This results in the following two main questions:

1) Can time-resolved dosimetry be performed based on MR-LINAC log-files?
2) Is logfile based dose reconstruction an accurate method for QA?

Since we are using the Delta4 phantom+ MR to measure the physical doses, the sub-question is:

3) Can the Delta4 phantom+ MR measure dose distributions at small time-intervals?

For both methods we are interested in the limitations, therefore the second sub-question is:

4) What are the limiting factors in logfile based dose-reconstruction and dose measurements using the Delta4 phantom+ MR at a small time-interval.

In final part of this thesis we will translate the results towards clinical practice and the future.

2. Materials and Methods

2.1 MR-LINAC

All experiments were performed on the clinical Elekta Unity MR-linac systems (Elekta AB, Stockholm, Sweden) equipped with a Philips Marlin 1.5T MRI scanner (Philips Healthcare, Best, the Netherlands) and 7 MV FFF (Elekta, Crawley UK) accelerator. The MRI part is based on the wide bore 1.5T Ingenia system, but with modifications for compatibility with a linear accelerator (figure 4). A ring gantry, which holds all the beam generating components, such as the magnetron, waveguide, a standing wave linear accelerator, and the Multi Leaf Collimator (MLC), is positioned around the cryostat. The active shielding of the magnet has been changed to create a torus of near zero magnetic field around the magnet at the location of the sensitive electronic components, waveguide, and the gun of the Linac. The system is equipped with a 2 x 4 channel radiolucent receive array (coil), with electronic components placed outside the radiation window to minimize attenuation and radiation induced currents that may impact image quality [5]. The source-axis distance (SAD) of the MRL is 143.5 cm. The MLC is equipped with 80 leaf pairs of 0.72 cm width, which travel in the cranio-caudal direction. The dose maximum of this beam is at 13 mm depth. The linac was calibrated to deliver 1 Gy per 100 MU at dose maximum, according to the NCS-18 Code of Practice [19].

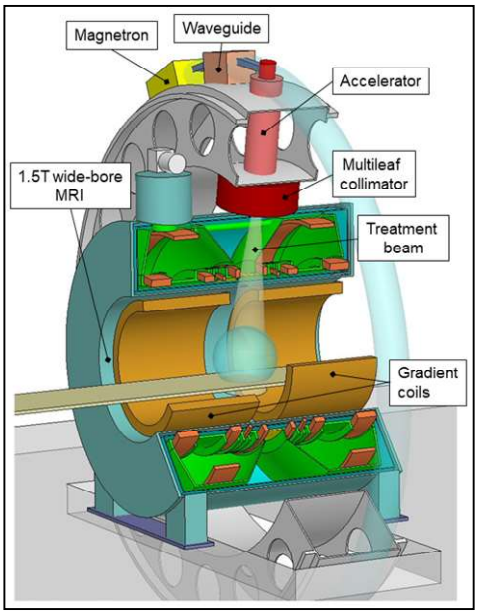

Figure 4 - Schematic diagram of the MR-LINACs internals.

2.2 Treatment planning system - Monaco

The Monaco® treatment planning system (TPS) (Elekta, Stockholm, Sweden) version v5.40.01 was used for creating the RT-plans. Monaco utilizes a GPU-based Monte Carlo dose (GPUMCD) calculation algorithm that takes into account the effect of the magnetic field on the dose distribution during the planning stage [20].

Particles arising from the source model are transported directly to the surface of the patient model. Next, Monte Carlo (MC) techniques are used to transport the radiation through the patient model and to calculate the deposited dose. This dose calculation is based on 'stopping-power-ratios' and "attenuation coefficients" originating from the material properties of tissues. Physical densities are determined analytically from the relative electron densities in each dose voxel. During the time that particles lose energy in the patient model, a low energy cutoff is used to terminate calculations when the particle's expected path length is smaller than a common dose voxel size [21]. The statistical uncertainty in the MC calculation is approximated from a series of calibration calculations and scaled within the dose distribution. For our dose distributions a statistical uncertainty of 0.25% and a grid spacing of 3 mm was selected. The Monaco dose distributions were exported for the total plan or per beam in the DICOM-RT format and used as input for the Matlab software (see section 2.7).

2.3 Treatment plans

Two RT treatment plans, created with Monaco, were chosen for validation and analysis. Both RT plans use step-and-shoot intensity modulated radiotherapy (IMRT) and magnetic resonance (MR)-based treatment planning. The first RT plan is simple and short with a fixed set of variables, whereas the second RT plan is more complex. In this way we assessed the response of the system in a simple configuration and clinical setting.

The first plan is a 4-field RT box plan with a rectangular shape of 10x10 cm, a dose rate of 411 MU/min and a cumulative dose of 3200 MU per field. The gantry angle of the 4 fields are 45, 135, 225 and 315° (figure 5). The dose rate, cumulative dose per field and field size are fixed, while each field contains 1 segment.

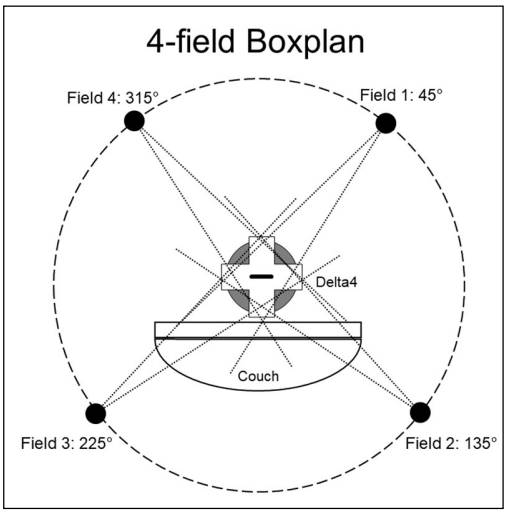

Figure 5 – RT box plan consisting of 4 fields and a squared shape of 10x10 cm.

Secondly, the patient RT plan was randomly selected in a list of patients who were treated on the MR-LINAC. The plan was created by the radiotherapist and used for irradiating a esophagus carcinoma. This plan has 7 fields and a total of 57 segments. The dose rate and field shapes vary over the treatment plan (see table 1).

Table 1 – 2D dose distribution for the patient RT-plan in the coronal plane with varying field shapes.

Beam no.	1	2	3	4	5	6	7
2D dose distribution per beam in the coronal plane	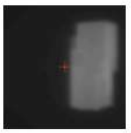			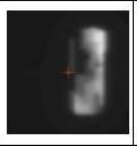	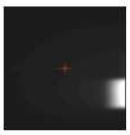	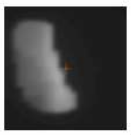	

2.4 Logfile dose reconstruction

For the logfile dose reconstruction, the standalone Elekta dose calculation engine was used. This engine, Graphical Processing Unit Monte Carlo dose (GPUMCD), is an adaptation of the CPU-based XVMC [20]. GPUMCD has actually the same physics as XVMC and gains calculation speed by operating on a graphics processing unit (GPU). The GPUMCD patient model is created using the same methodology as described for XVMC. The particle generation source model of XVMC is used in GPUMCD and particle transport is nearly identical. However, there are two differences: 1. GPUMCD was developed to support particle transport in a magnetic field to accurately model electron motions in the MRI-LINAC. 2. GPUMCD calculates real statistical uncertainty in the dose voxels.

GPUMCD requires three inputs, namely the RT-plan, logfile and a CT scan. The logfile contains the machine parameters of the MR-LINAC during radiation delivery, like MLC/gantry positions, table position and dose rate. All parameters are saved per 40ms (25 Hz) and stored in a binary TRF-file. The TRF file was converted to a tabular CSV format, split every 200ms and saved to a new file. Only the files with a dose rate > 0 MU were selected as input for GPUMCD. Another important input for GPUMCD is a CT scan to assess electron density required for calculations. We used a static artificial created CT with a slice thickness of 1 mm, which represents the geometry of the Delta4. An statistical Monte Carlo uncertainty of 8% per segment/control point for the partial dose calculations was used. The calculations

were performed on Intel Xeon based workstations with at least 32GB RAM and Nvidia GTX Titan cards. The logfile based dose distributions per 200ms were saved in the DICOM-RT format and used as input for the matlab software (see section 2.7).

2.5 Delta4 – Hardware and setup

For physical dose measurements we use an MR compatible phantom. The Delta4 Phantom+ MR is an adapted Delta4 PT phantom to be compatible with MR-Linacs and consists of cylindrical polymethyl-methaacrylate (PMMA) containing 2 orthogonal detector boards (200 x 200 mm) with in total 1069 p-type Si-diodes (Scandidos), see figure 1. The p-type cylindrical silicone diodes have an active volume that is 1 mm in diameter and 0.05 mm thick [22].The sagittal detector plane has 561 diodes with a centered high diode-dense area (5 mm spacing) and an outer low diode-dense area (10 mm spacing). The coronal detector plane has 508 diodes with two smaller high diode-dense areas (5 mm spacing) and an low diode-dense area (10 mm spacing).

For setup, the cylindrical phantom has double-line crosshairs inscribed on three sides and leveling screws on four corners. The double lines are 1.5 mm apart, and the phantom position is adjusted until the room lasers fall between these lines.

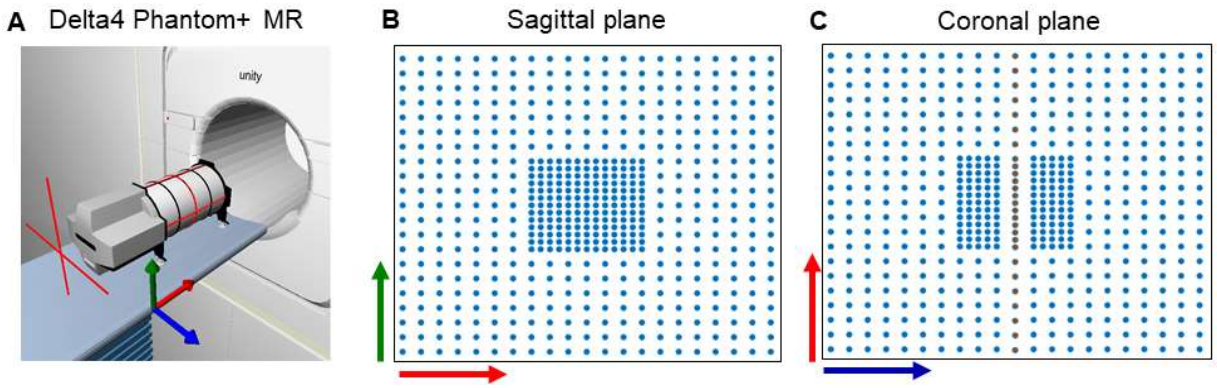

Figure 6 – 3D representation of the Delta4 Phantom+ MR from Scandidos (A) with 1069 detectors in the sagittal (B) and coronal plane (C).

2.6 Delta4 - Software

After setup and positioning, a power and data cable were connected to the Delta4 phantom. The data cable is connected to a dedicated PC which runs a software package from Scandidos. All diodes are read out simultaneously every approximately 0.150 ms. If the integrated signal is below a certain threshold, the recorded values are discarded. A signal above the same threshold means that a dose pulse is detected and recorded values are saved. The current setup of the board has a delay between pulses in the order of 0.150 ms.

For this project, Scandidos supplied us with a research version of their software in order to export the raw diode dose values. The exported file is a tabular CSV format with the XYZ-positions of the detectors and dose values from each diode, recorded every 25 ms (40 Hz). The recorded values contains the integrated signal from all pulses within 25 ms. A time stamp is set 25 ms after the arrival of the first pulse in each package. The exported CSV files are used as input for the Matlab software (see next section).

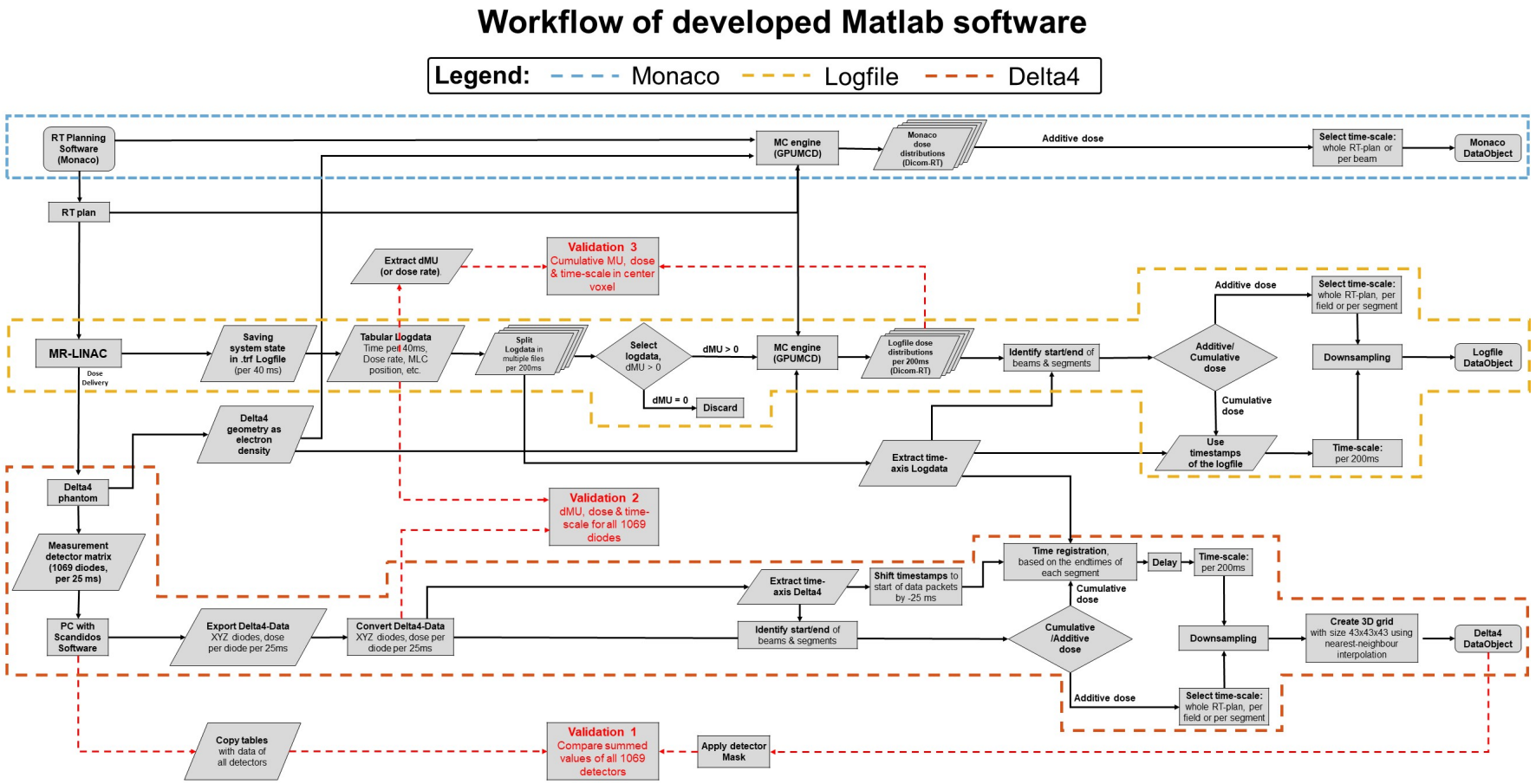

Figure 7 - The workflow of developed Matlab software for the 3 types of dose distributions: 1. Monaco (blue). 2. Logfile (yellow) 3. Delta4 (orange). Three validation experiments were performed, highlighted in red.

2.7 Matlab Software

For comparison of the Monaco, Logfile and Delta4 dose distributions, a program was written in Matlab (version R2019a, Natick, Massachusetts: The MathWorks Inc.). An in-house developed Matlab framework, used for film QA, was adopted for structuring the data and automating basic processes. Three workflows were created (figure 7): 1. Monaco 2. Logfile 3. Delta4. The final software outputs multiple dose distributions at different time points wrapped into a single DataObject. The dose values in the DataObject can be stored additively, meaning that the dose values are saved per selected time scale, or cumulatively, meaning that the dose values are saved as a cumulative sum of preceding dose values. In the Monaco workflow, the DICOM-RT files were imported, stored in an additive manner and either saved as a total plan or per beam. In the Logfile workflow, the DICOM-RT files per 200ms were imported, stored in an additive or cumulative manner and downsampling was performed based on the selected time-scale. For the Delta4 workflow, the CSV files were imported and saved in an additive or cumulative manner. Downsampling was performed based on the selected time-scale and a 3D grid was created using nearest-neighbor interpolation.
The validation of the software will be discussed in the next section, whereas the time-synchronization is discussed in section 2.9.

2.8 Validation

In the evaluation experiments the consistency of the datasets and the correct working of a specific part of the system was checked (see figure 7, highlighted in red). Three validation experiments were performed: 1. Check of the detector values in the Delta4 DataObject. 2. Consistency of time-axis & dose values in the RAW logfile and Delta4 export files. 3. Consistency in the Logfile based dose reconstruction. In validation experiments 1 and 2, both the box and patient RT-plan were used, whereas in the last experiment only the box RT-plan was used.

2.8.1 Detector values in Delta4 DataObject

Here, we validated the detectors values in the Delta4 DataObject by comparing the sum of all 1069 detector values with that of the Scandidos software. In the Scandidos software, under the “tables” dialog, cumulative numerical data for all detector positions (in both detector planes) was available, specified to two decimal points. Detector values in the Delta4 DataObject were based on exported CSV files, which lists the dose values per detector, specified to 14 decimal points on a timescale per 25ms.

2.8.2 Time-axis and dose values

The second validation experiment concerned the dose values and time-axes from the logfile and Delta4 CSV-files. In the logfile, several variables are present that report the dose in motor units (MUs). These can be used for indicating if the radiation is turned on or off. An MU is a dose counter unit of the dose monitor of the linac. MU is related to the dose delivered at isocenter under certain conditions. The following 3 variables are available in the logfile of the MR-Linac: 1. Actual Dose Rate/Actual Value 2. Step Dose/Actual Value 3. Dose/Raw value. The actual dose rate is the current step dose in MU/min, whereas the step dose is in MU. The Dose/Raw value is the current segment dose as reported to the agility control system by the linac control system in 1/64th MU.
In the logfile, each timestamp represents the status of the machine during a 40ms interval, e.g. if the timestamp is 2.2 sec then that row describes the status between 2.2 and 2.24 seconds.

In the Delta4 CSV-file, all dose values per diode are stored, but only when the cumulative dose of all the diodes is above a certain threshold. The data packages contains the integrated signal from all pulses within 25 ms. The time stamp is set 25 ms after the arrival of the first pulse in each package.
After importing the Delta4 CSV-file, we changed the timestamps of the Delta4 to the beginning of a data package, similar to the logfile timestamps. As for the dose, we compared the duration of a segment, recorded by the Delta4, with that to the 3 dose parameters in the logfile. We chose the dose parameter that best fits the duration of the fields/segments of the Delta4. The selected dose parameter in the logfile is plotted in a graph along with the raw output from the Delta4 export files.

2.8.3 Cumulative calculated dose

In the third validation experiment we compared the cumulative MUs (from logfile) with the calculated dose in the center voxel after dose reconstruction with GPUMCD. We convert the dose rate (MU/min) into the amount of MU per 40ms and took the cumulative sum of all Mus per field.

2.9 Time-synchronization

Synchronization in the time domain is crucial for a good comparison of different dose distributions. Time synchronization was straightforward for the time-scales: per field and per segment, since a time period of non-irradiation occurred between each consecutive part, see figure 8.

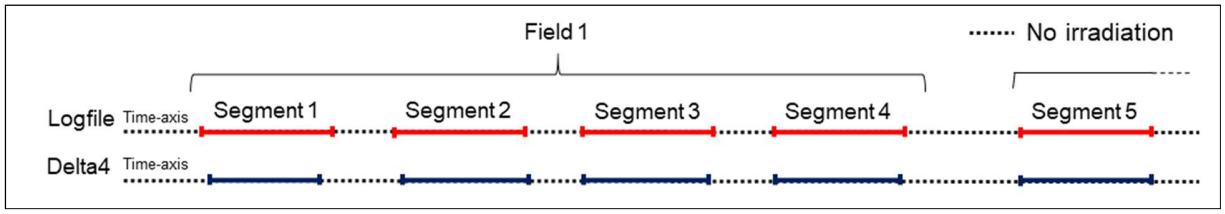

Figure 8 – Schematic representation of the Logfile and Delta4 time-axis (not synchronized) with periods of irradiation (red and blue) and non-irradiation (dashed line).

For the time-scale per 200ms, synchronization of the two dose distributions was performed on the last 200ms frame of each segment. First, a delay was calculated resulting in the alignment of t_1 and t_2, then resampling of the Delta4 data was performed starting at the end towards the beginning of the segment (figure 9).

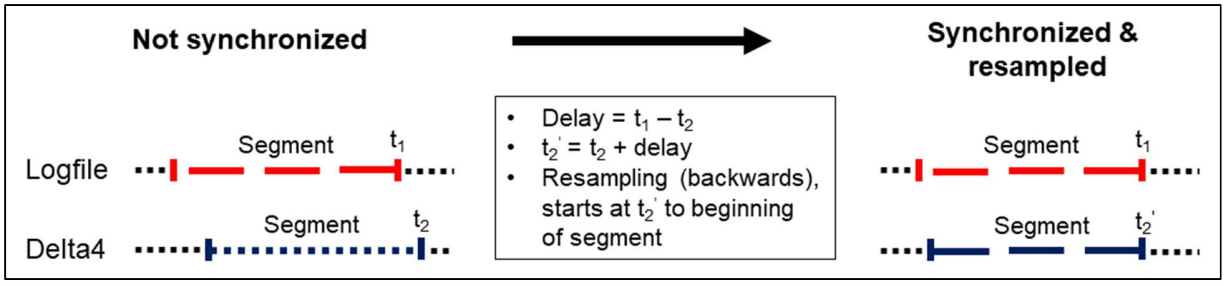

Figure 9 – Schematic representation of the Logfile and Delta4 time-axis before synchronization and after with periods of irradiation (red and blue) and non-irradiation (dashed line).

2.10 Analysis

In our analysis we compared the reference and the target DataObjects (figure 10). For the reference DataObject we had the option for selecting the Monaco or Logfile DataObject. In the Monaco dataset only the total RT-plan and per field timescales were available. For the target, the logfile and Delta4 DataObject were available for selection. Next, transformations were applied so that the final distributions have the same characteristics. If the Delta4 DataObject was selected as a target, a mask was applied, so that only the dose values corresponding to the detectors locations were selected. Qualitative and quantitative tools for performing the analysis were implemented: 1. Visual inspection 2. Dose profile 3. Dose Difference 4. Gamma-index.

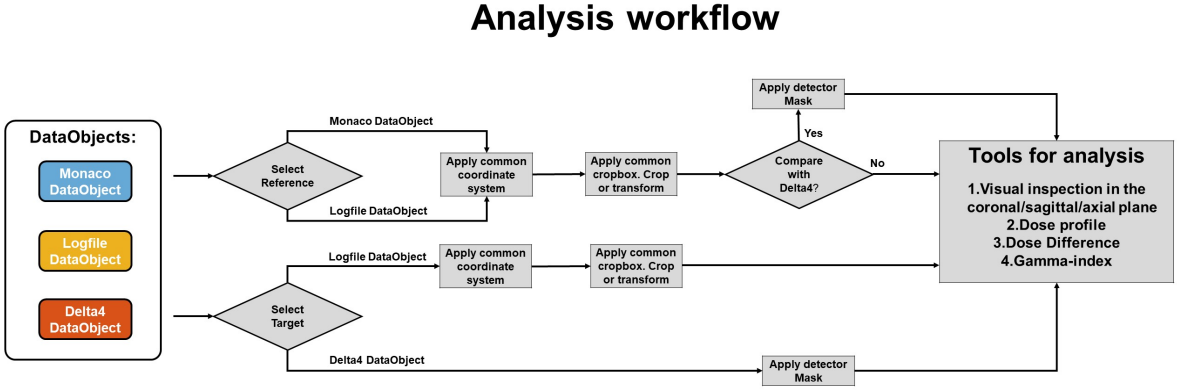

Figure 10 – Analysis workflow for comparing the different DataObjects.

2.10.1 Qualitative

A 2D colorplot was made in the center of the dose distributions in the coronal, axial and sagittal plane. The absolute differences between the two planes were plotted on a colorscale. For comparison with the Delta4, only the coronal and sagittal plane were used, since the Delta4 lacks an axial detector plane. Also dose profiles were used for both dose distributions, which is a drawn line on a selected plane resulting in a 1D graph with length and dose. Visual inspection of the lines give an estimate about the correspondence of the dose distributions.

2.10.2 Quantitative - Dose Difference

Dose difference (DD) is a comparison of dose at corresponding location in two dose distributions [23]. The absolute dose difference is defined as:

$$DD = D(a_m) - D(a_p) \tag{1}$$

were $D(a_p)$ is a the dose in the planned distribution and $D(a_m)$ is the dose in the measured distribution at the corresponding location. Also a relative dose difference can be calculated, defined as:

$$DD = \frac{D(a_m) - D(a_p)}{D_{norm}} \tag{2}$$

were $D(a_p)$ and $D(a_m)$ are the doses in the two dose distributions at the corresponding location. The normalization factor is D_{norm} and is defined as the average over the 6 highest voxel values per timescale in the selected reference dose distribution.

A passing criterion is used, e.g. 3% of planned dose, such that if the measured dose difference is <= 3% the measured distribution "passes" at that point. The drawback of the dose difference test is that it is not robust in high gradient regions, as small misalignments can cause large dose differences.

2.10.3 Quantitative – Gamma-index

The gamma-index is an combined measure of the DD and the distance to agreement (DTA). The DTA is given by the nearest point in the measured distribution [23], such that:

$$D(a_p) = D(a_m + r) \tag{3}$$

were a_p is a point in the planned distribution, a_m the corresponding point in the measured distribution and r is the calculated distance in mm to meet the above criteria. In DTA also a passing criterion is chosen, e.g. 5 mm. If the matching dose level is found within a radius of <= 5 mm, the measured distribution "passes" at that point. This technique is robust against misalignments in high gradient regions. However, this technique is prone to failure in low gradient regions, where even small misalignments can require a large radius to find the matching dose level.

The gamma-index combines DD and DTA into a metric resembling a distance (Eq. 4) [24]. In this way both dose difference and DTA are taken into account for every point compared.

$$\Gamma = \sqrt{\frac{d_{DTA}^2(r_a, r_b+r)}{\delta_{DTA}^2} + \frac{|D_a(r_a) - D_b(r_b)|^2}{\delta_{DD}^2}} \tag{4}$$

were $D_a(r_a)$ is a dose in the first distribution at point r_a, and a $D_b(r_b)$ is a dose at the corresponding point r_b in the second distribution. The DTA condition (first part of formula XX) is fulfilled when $D_a(r_a) = D_b(r_b+r)$, where r is an arbitrary point a distance $|r|$ away from r_b, whereby δ_{DTA} is used as a threshold passing value. The DD (second part of formula XX) is the difference of the two doses at the corresponding points: $|D_a(r_a) = D_b(r_b)|$, with δ_{DD} as an pass/fail threshold. Both δ_{DTA} and δ_{DD} are used to normalize the result in the gamma equation.

The actual gamma index γ, is determined by finding the minimum value of Γ by varying r, given by

$$\gamma(r_a, r_b) = min\{\Gamma(r_a, r_b), \forall r\} \tag{5}$$

This actual means traveling along the isodose contour and finding the point at which DTA is smallest. The convention is for passing γ to be ≤ 1 and failing to be > 1. The gamma-index provides a single value for evaluation, rather than using two separate tests and considering both.

We used the Matlab implementation of the gamma-index by Geurts et al. [25], this method was proven to be reliable [26]. Gamma criteria with DD of 3, 2 and 1 % and a DTA of 3, 2 and 1 mm were calculated in the analysis. In general, a passing rate of 90% and above for the gamma index (DD=3% and DTA=3 mm) was considered acceptable [27], [28].

3. Results

3.1 Validation

This section contains the result for consistency verification of the datasets and the correct working of the developed software. Each paragraph represents a validation experiment, see figure 7 (highlighted in red).

3.1.1 Detector values in the Delta4 DataObject

The detector values in the Delta4 DataObject are verified by comparing the sum of all detector values in the DataObject with those from the Scandidos software. Table 2 summarizes the summed diode values and differences for the box RT-plan as a total and per field. The maximum absolute difference is 0,24 mGy.

RT-Plan: Box	**Summed diode values (in mGy)**		**Difference (in mGy)**
	Delta4 software	**DataObject**	
Total plan	57026.69	57026.93	0.24
Field 1	12934.34	12934.48	0.14
Field 2	15667.56	15667.61	0.05
Field 3	15452.71	15452.67	0.04
Field 4	12972.08	12972.17	0.09

Table 2 – Summed dose values of 1069 diodes in the Delta4 software and DataObject with difference, performed for the box RT-plan.

The results for the patient RT-plan are summarized in figure 11. The shapes of the histograms of the Sandidos software (figure 11A) and DataObject (figure 11B) are the same , whereas the summed values of all diode values differ by 0,07 mGy.

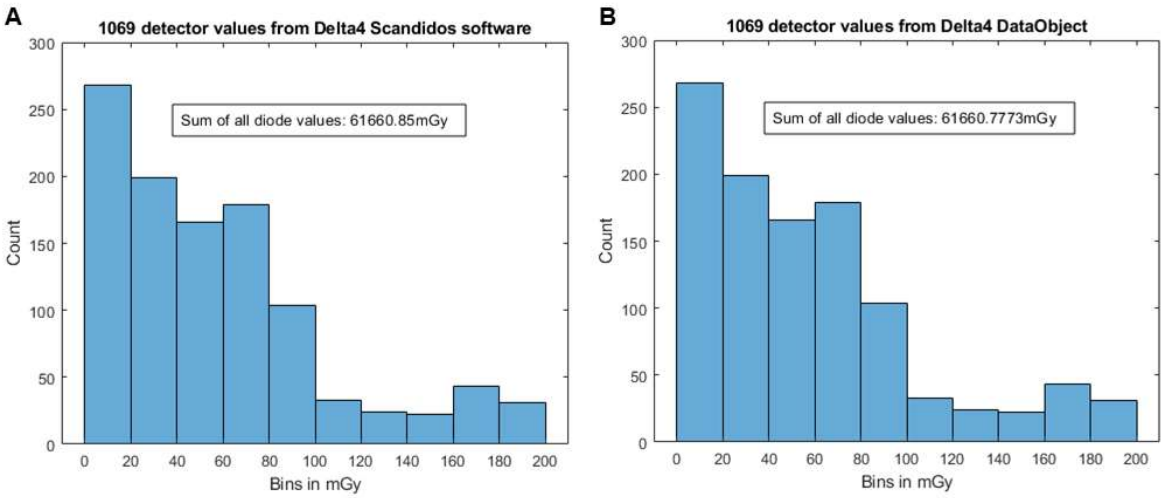

Figure 11 – Histogram of 1069 Delta4 detector values for Scandidos software (A) and the DataObject (B), including summed value (lined box) for patient RT-plan.

3.1.2 Time-axis and dose values

There is a difference in duration of the fields/segments in the RT-plans between the logfile and Delta4 data. In the Delta4 data we can select only 1 dose variable, whereas in the logfile data 3 dose variables are available. In table 3, the length per field for the different does variables are summarized using the box RT-plan. For fields 1,2 and 4, the actual dose rate has the best match with the Delta4 regarding the lengths of the fields.

Table 3 – Time lengths from the logfile (3 dose variables) and Delta4 with their differences using the box RT-plan consisting of 4 fields.

RT-Plan:	**Logfile – length of fields in ms for**			**Delta4 – length of fields in ms**	**Difference Delta4-ADR in ms**
BOXPLAN	**Actual Dose Rate (ADR)**	**Step Dose**	**Dose**		
Field 1	7040	7160	7160	7087	47
Field 2	7000	6960	6960	7111	111
Field 3	6920	7000	7000	7037	117
Field 4	7040	13480	13480	7062	22

For the patient RT-plan, the time differences of 57 segments are plotted in figure 12. The timestamps of the Step dose and Dose were similar, resulting in the same histogram (figure 12A). The Step Dose/Dose has a median of -102 ms, a minimum value of -296 ms and a maximum value of 62 ms. In figure 12B, the difference in length of the segments between the Delta 4 and logfile parameter Actual Dose Rate is plotted. It has a median of 2 ms with a range of -114 to 121 ms. The parameter "Actual Dose Rate" was selected in further analysis, since it had the lowest time differences.

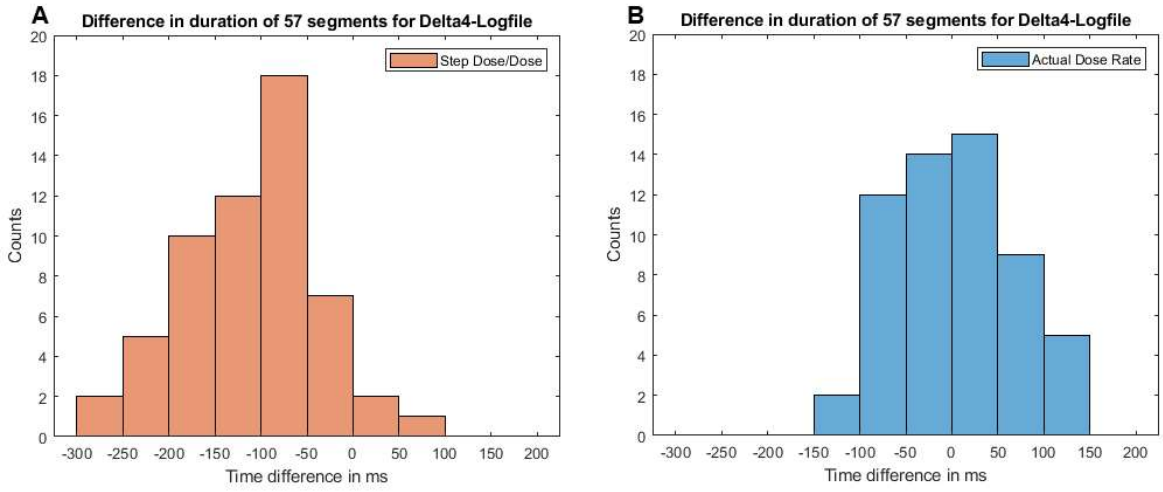

Figure 12, Histogram of time differences in duration of segments between Delta4 and Step Dose/Dose (A) and actual dose rate (B).

In the comparison of the actual dose rate (from the logfile) and dose output (from the Delta4), only detectors of the Delta4 are selected within the field of irradiation. This is performed by selecting detector values with a cumulative dose of more than 800 mGy (>75% of the maximum), resulting in a selection of 454 detectors. In figure 13 we can identify the 4 fields of the box RT-plan. The actual dose rate of the logfile is roughly the same for the 4 fields. The sum of Delta4 detector values in the two middle fields are lower in comparison to the first and last field. This can be explained by attenuation, caused by the treatment table. Moreover, there is a bandwidth of about ± 50 Gy where the sum of the

Delta4 detector values fluctuates between. These fluctuations can partly be explained by the fact that the length of each data packet is not the same (± 0.1ms). This behavior can also be caused by electrical noise.

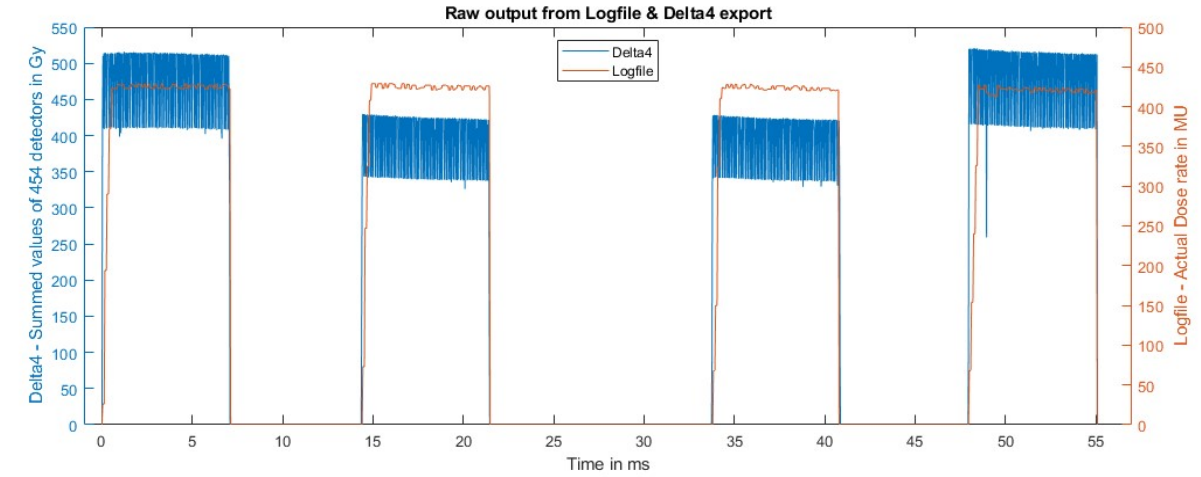

Figure 13 – Raw output of the Logfile & Delta4 export files. The actual dose rate in MU (orange line) and the summed dose values of the selected Delta4 detectors in Gy (blue line). Please note that summed dose values (blue line) of fields 2 & 3 are lower because of attenuation, caused by the treatment table.

3.1.3 Cumulative calculated dose per field

Here, we compare the cumulative MUs (from the logfile) with the calculate dose in the center voxel after dose reconstruction with GPUMCD, each with its own time-axis. We use the box RT-plan, consisting of 4 fields over a time period of about 55 s (figure 14).

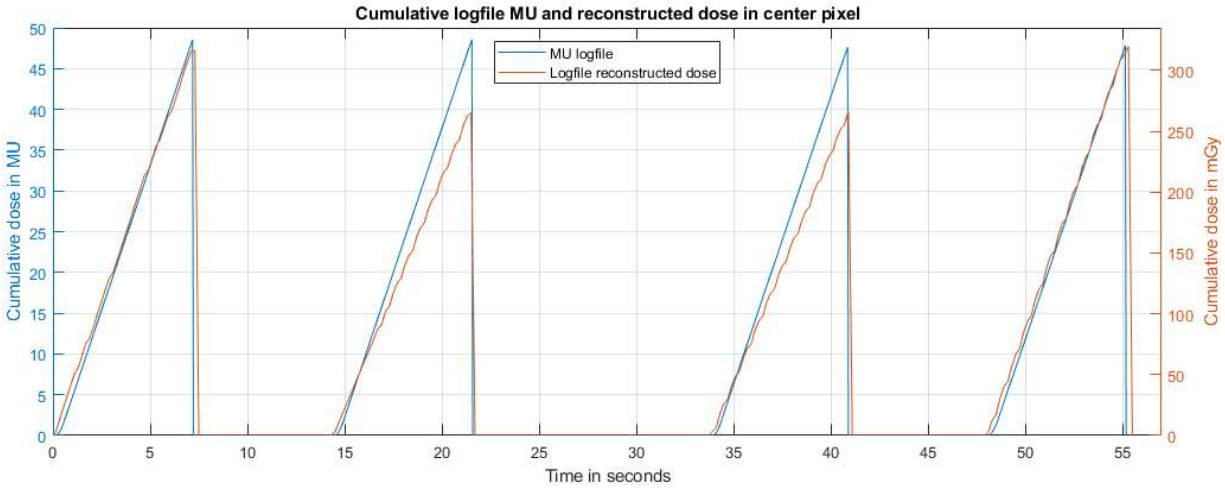

Figure 14 – Comparison of the cumulative MUs (blue line) from the logfile with the reconstructed dose in the center voxel (orange line). Please note that the dose values (orange line) of fields 2 & 3 are lower because of attenuation, caused by the treatment table.

3.2 Time-synchronization

For the box RT-plan we identified the 4 fields, each consisting of 1 segment, by the time-interval of non-irradiation. The non-irradiation time between the fields 1-2, 2-3 and 3-4 were respectively 7000, 12200 and 7000 ms.

The patient RT-plan consisted of 7 fields and a total of 57 segments. The non-irradiation time between two consecutive segments is displayed in figure 15. Six segments had a time-interval of > 5400 ms and were identified as transition times from the end of a field to the beginning of a new field (figure 15, purple bars). The other time-intervals were between consecutive segments (figure 15, blue bars).

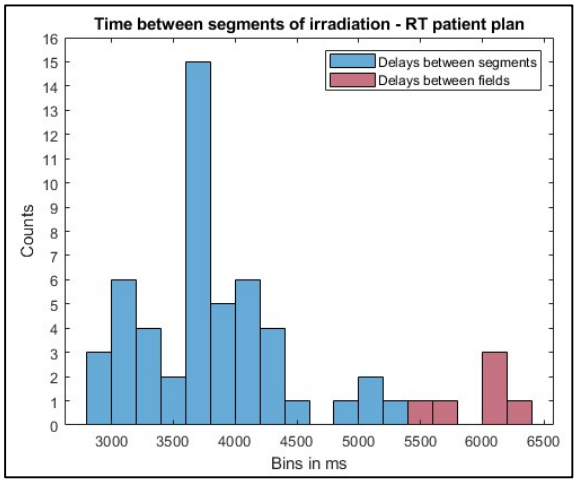

Figure 15 - Histogram of time-intervals between segments (blue bar) and fields (purple bar) for the patient RT-plan.

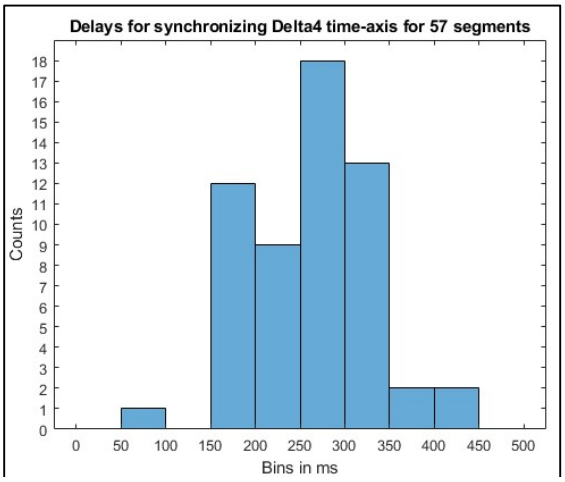

Figure 16 – Delays of 57 segments required for sub-segment time synchronization between the logfile and Delta4.

Synchronization on a sub-segment scale was based on alignment of the ends of each segment (see figure 17). Delays were calculated for 57 segments (see figure 16) and were used for correcting the timescale of the Delta4 (see figure 17B-C).

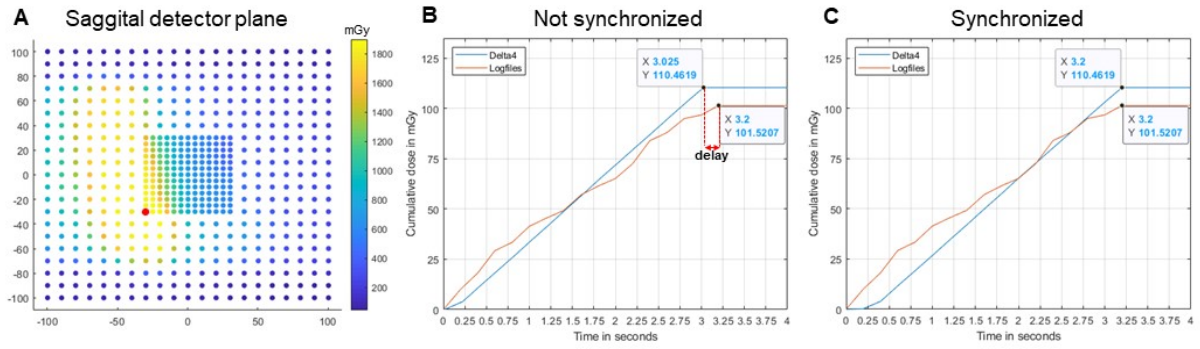

Figure 17 – Example of the cumulative dose in one detector point (A) measure by the Delta4 (blue line) and logfile reconstruction (orange line), before(B) and after (C) synchronization for the patient RT-plan.

3.3 Analysis

Here we present the results of compared DataObjects using the patient RT-plan.

The results of the Monaco – Logfile comparison are covered in paragraph 3.3.1 and 3.3.2. The results of the Monaco - Delta4 comparison mirrors the outcome of the Scandidos software, see Appendix A. The results of the Logfile – Delta4 comparison are covered in paragraph 3.3.3 to 3.3.6.

3.3.1 Monaco & Logfile – Total RT-plan

Here,, we will compare the Monaco and the logfile dose distribution for 2 timescales: cumulative (this paragraph) and per beam (paragraph 3.3.2).

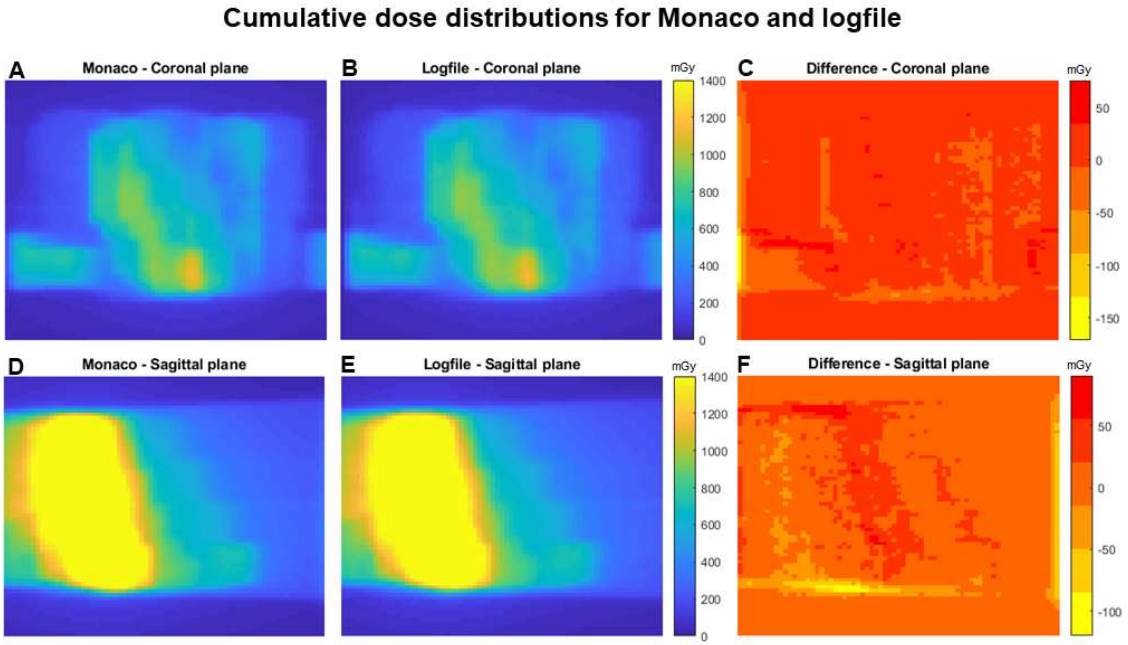

Figure 18 – Cumulative dose distribution for Monaco (A & D) and logfile (B & E) with difference (C & F) in the coronal (A-C) and sagittal plane (D-F).

Figure 18 shows the cumulative absolute dose for the two distributions in the coronal and sagittal plane. The maximum dose differences in the order of -50 to 50 mGy are observed in the center of the coronal plane. In the sagittal plane, maximum dose differences of -100 up to 100 mGy are observed, particular near the upper and lower borders of the high dose area.

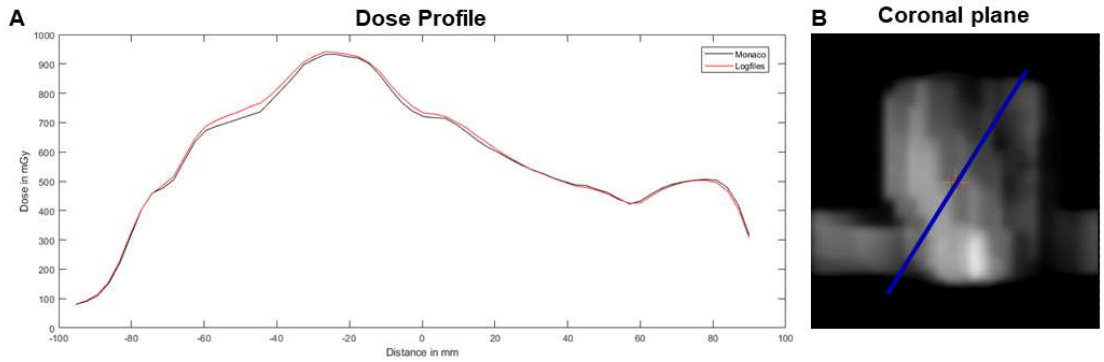

Figure 19 –Dose profile (A) of a diagonal line in the coronal plane (B) in the Monaco (black line) and logfile (red line) dose distribution.

The dose profile of the Logfile follows the Monaco dose line closely, see figure 19.
The relative dose difference and gamma-index for the Monaco and Logfile dose distribution is plotted in figure 20. All voxels in the distribution are taken into account. The median is 0% and the borders for 90% of the data are located between a dose difference of -1.5 and 1.5 %. Dose differences of -5.4 and 4.6% are the ranges for 99% of the data.
For DD=3% and DTA=3mm: In 90% of the data, a maximum gamma-index of 0.30 was observed, while 99% of the data a maximum gamma-index of 0.90 was noted.
For DD=2% and DTA=2mm: In 90% of the data, a maximum gamma-index of 0.44 was observed, while 99% of the data a maximum gamma-index of 1.35 was noted.
For DD=1% and DTA=1mm: In 90% of the data, a maximum gamma-index of 0.89 was observed, while 99% of the data a maximum gamma-index of 2.0 was noted.

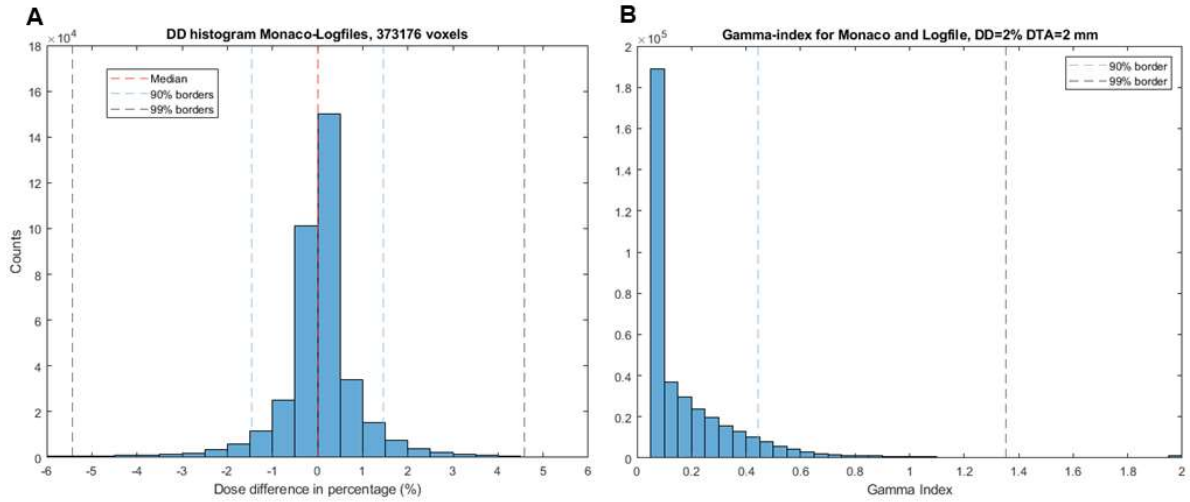

Figure 20 – Dose difference (A) and Gamma-index (B) for Monaco and Logfile dose distributions, including median (red line), 90% borders (blue lines) and 99% borders (black lines).

3.3.2 Monaco & Logfile – per beam

In this section we will discuss the results of the Monaco and logfile distribution per beam.
The relative dose difference per beam is shown in figure 21. The median for all the beams is near 0 %, whereas the range for 90% of the data, considering all beams, is -3.3 to 2.4%. The range which includes 99% of the data is -7.7 and 13.8%, taking into account all beams.

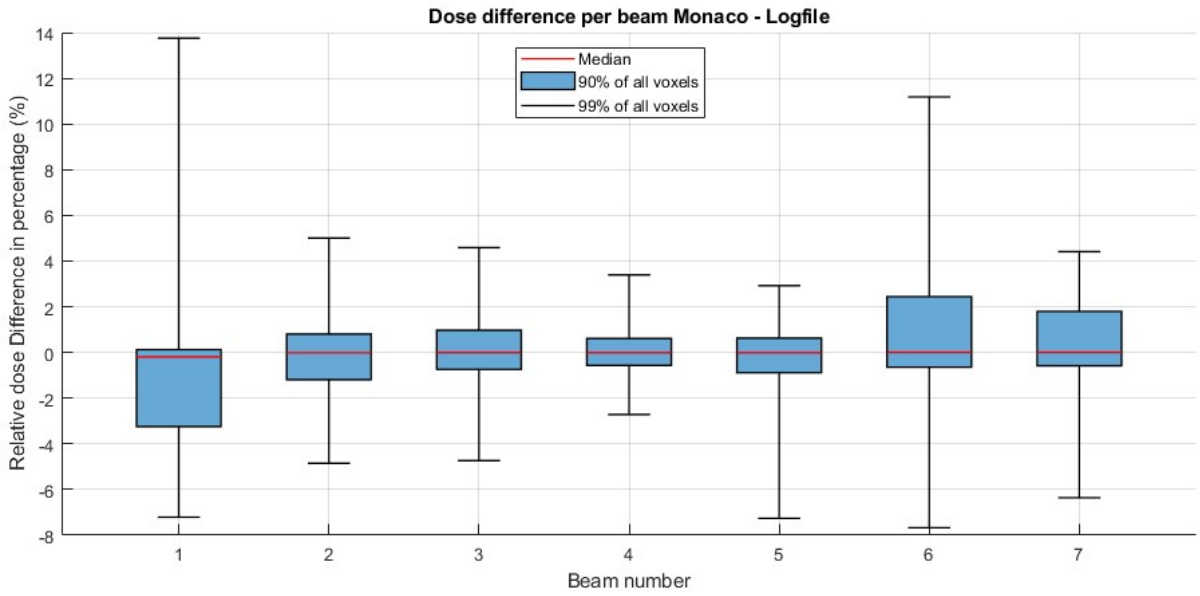

Figure 21 – Boxplot of the dose difference for 7 beams with the median (red line), 90% of the data (blue bar) and 99% of the data (whiskers).

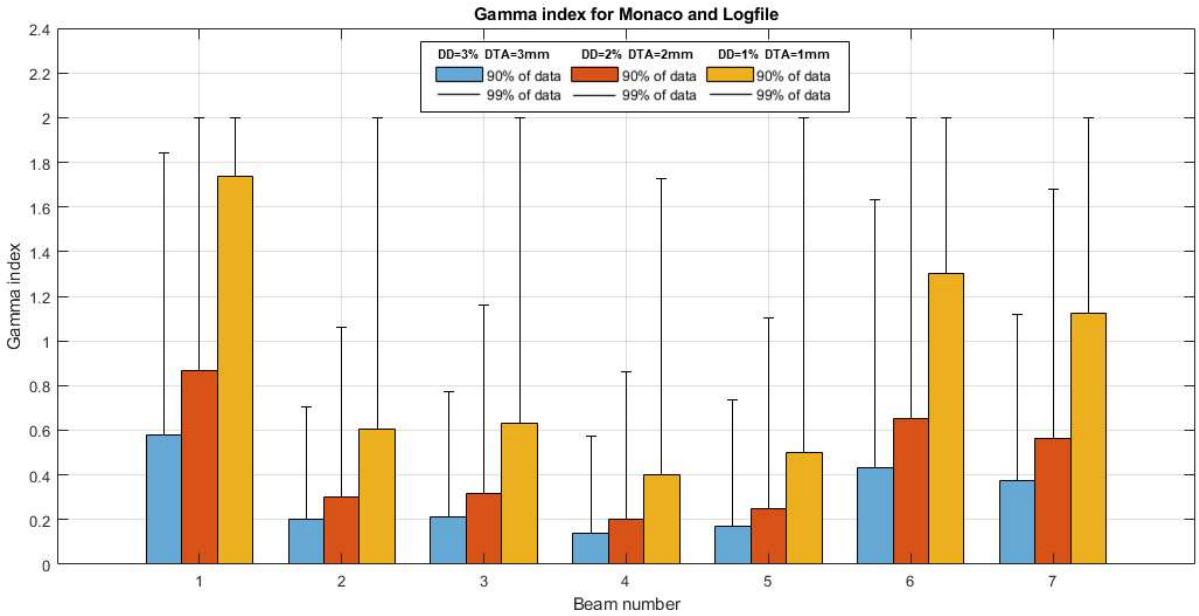

Figure 22 – Gamma index for Monaco and Logfile using DD of 3, 2 and 1% and a DTA of 3, 2 and 1 mm, displaying 90% of the data (blue bars) and 99% of the data (whiskers).

The gamma index for Monaco and Logfile dose distributions is shown in figure 22 for 373176 voxels. For the parameters, a DD of 3, 2 and 1% and a DTA of 3, 2 and 1 mm was chosen.
For DD=3% and DTA=3mm: In 90% of the data, a maximum gamma-index of 0.58 was observed, while 99% of the data a maximum gamma-index of 1.84 was noted.

For DD=2% and DTA=2mm: In 90% of the data, a maximum gamma-index of 0.87 was observed, while 99% of the data a maximum gamma-index of 2.0 was noted.
For DD=1% and DTA=1mm: In 90% of the data, a maximum gamma-index of 1.74 was observed, while 99% of the data a maximum gamma-index of 2.0 was noted.

3.3.3 Logfile & Delta4 – Total plan

Here, we will present the results of the comparison between the Logfile and Delta4 dose distributions on a timescale of: 1. Total RT-plan 2. per field 3. per segment 4. per 200ms.
Figure 23 gives a visual overview of the total RT-plan for the two dose distributions displayed in the coronal, axial and sagittal plane. The logfile distribution has a higher resolution than the Delta4 dose distribution. The contours in the Delta4 distribution are not sharp but resemble the logfile distribution in the coronal and sagittal planes. Since the Delta4 has no detectors in the axial plane, no dose information is available in this plane.

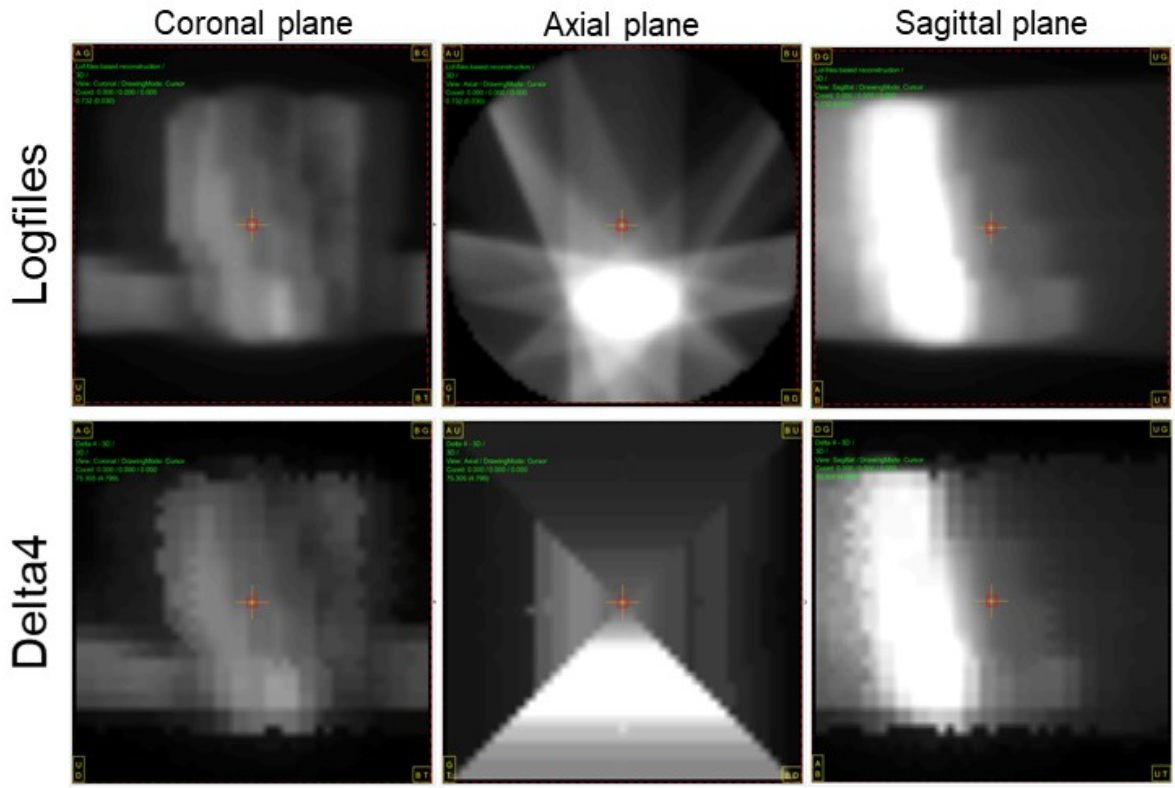

Figure 23 – Graphical representation of the logfile and Delta4 dose distrubtion for the patient RT-plan, viewed in the coronal, axial and sagittal plane.

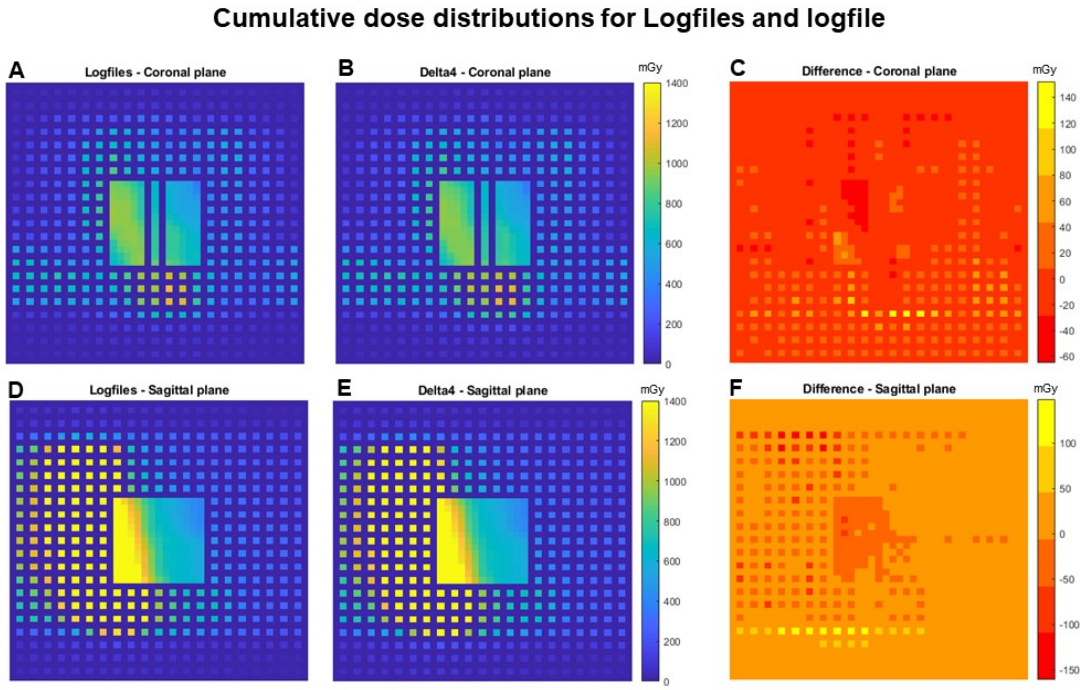

Figure 24 - Cumulative dose distribution of Logfile (A & D) and Delta4 (B & E) with difference (C & F).

In this experiment we will compare the Logfiles and the Delta4 readings on a cumulative timescale. Only the voxels that correspond to the locations of the 1069 Delta4 detectors are used.
Figure 24 shows the absolute dose measures per diode in the coronal and sagittal plane for the Logfile and Delta4. Maximal dose differences in the order of -60 to 140 mGy are observed in coronal plane. In the sagittal plane, maximum dose differences of around -150 up to 100 mGy are observed.

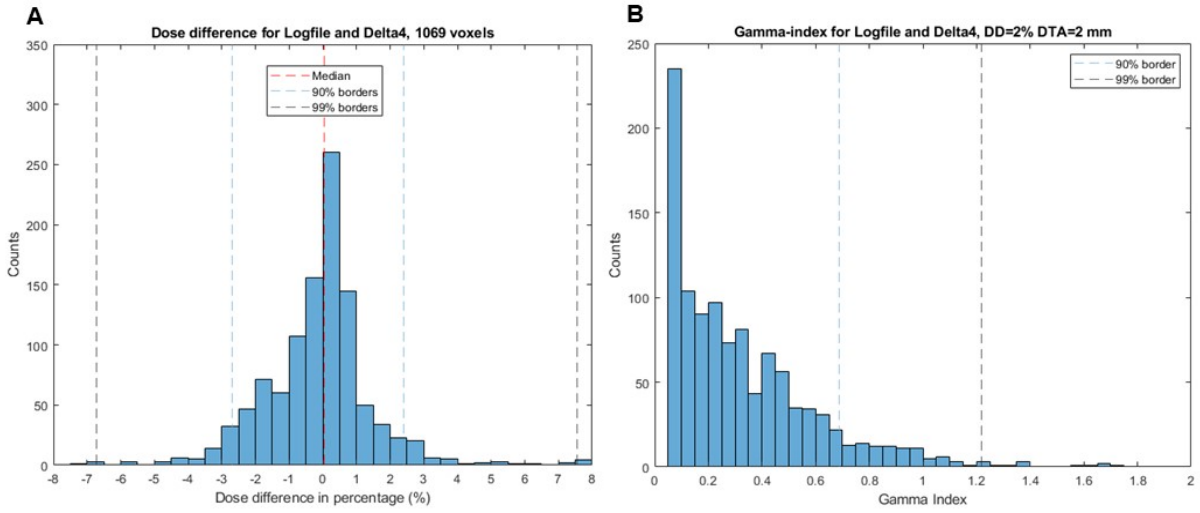

Figure 25 – Dose difference (A) and Gamma-index (B) for Logfiles and Delta4 phantom with 1069 detectors, including median (red line), 90% borders (blue line) and 99% borders (black line).

The dose difference between the Logfile and for the 1069 detectors of the Delta4 is plotted in figure 25A. A dose difference of -2.7 and 2.4% was found for 90% of the data and the range in dose difference

was -6.7 and 7.6% for 99% of the data. The gamma-index is 0.69 and 1.22 for respectively 90% and 99% of the data (figure 25B).

3.3.4 Logfile & Delta4 – per field

This section reports the results of the Monaco and Delta4 dose distribution per beam. Only 1069 voxels, related to the detector positions, are taken into account. The median dose difference is between -0.4 to 0.5% for all 7 beams (figure 26). The relative DD for 90% of the data (= 962/1069 voxels) is -4.7 to 2.5% considering all beams. In 99% of the data (= 1058/1069 voxels), the DD is between -8.7 to 8.2%.

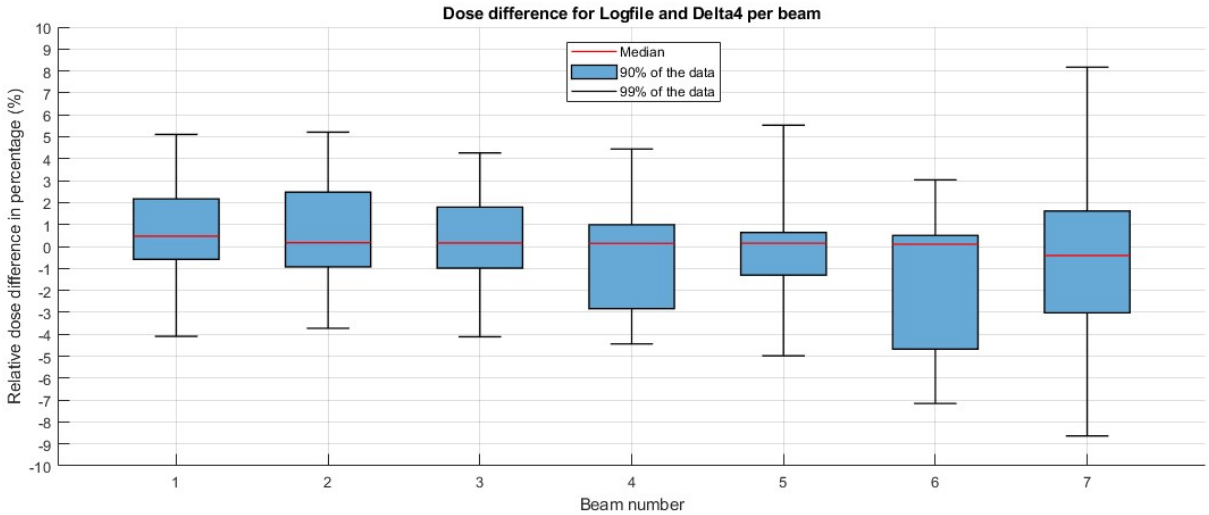

Figure 26 – Dose Difference for Logfile and Delta4 per beam, including median (red line), 90% of the data (blue bar) and 99% of the data (whiskers).

The gamma indices for Monaco and Delta4 dose distributions is shown in figure 27. For the parameters, a DD of 5, 3 and 1% and a DTA of 5, 3 and 1 mm was chosen.
For DD=3% and DTA=3mm: In 90% of the data, a maximum gamma-index of 0.66 was observed, while 99% of the data a maximum gamma-index of 1.38 was noted.
For DD=2% and DTA=2mm: In 90% of the data, a maximum gamma-index of 0.99 was observed, while 99% of the data a maximum gamma-index of 2.00 was noted.
For DD=1% and DTA=1mm: In 90% of the data, a maximum gamma-index of 1.99 was observed, while 99% of the data a maximum gamma-index of 2.00 was noted.

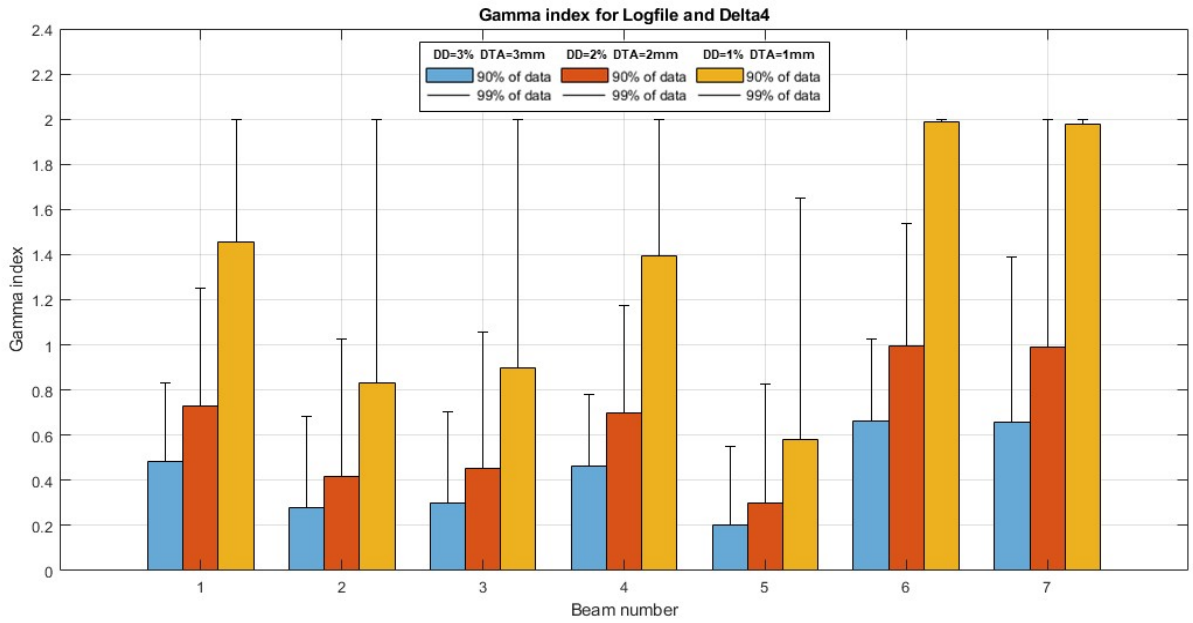

Figure 27 – Gamma index for Logfile and Delta4 using DD of 3, 2 and 1% and a DTA of 3, 2 and 1 mm, displaying 90% of the data (blue bars) and 99% of the data (whiskers).

3.3.5 Logfile & Delta4 – per segment

In this section we present the results of the log file and the delta4 dose distribution, containing a comparison of 1069 diode voxels on a 'per segment' timescale . Figure 28A shows boxplots of the relative dose difference for all 57 segments. The median DD, considering all the segments, has a range of -0.8 to 0.3 %. For 90% of the data, the range in DD is -5.9 to 6.0%. The DD values between -13.1 and 14.4% are for 99% of the data.

For all 1069 voxels, the gamma-index was calculated (with DD=3% and DTA=3mm) and the range is plotted in a bar chart covering 90% and 99% of the data (figure 28B). Selecting 90% of the data, the maximum value in gamma-index was 1.0, considering all beams, whereas for 99% of the data, the maximum value was 2.0.

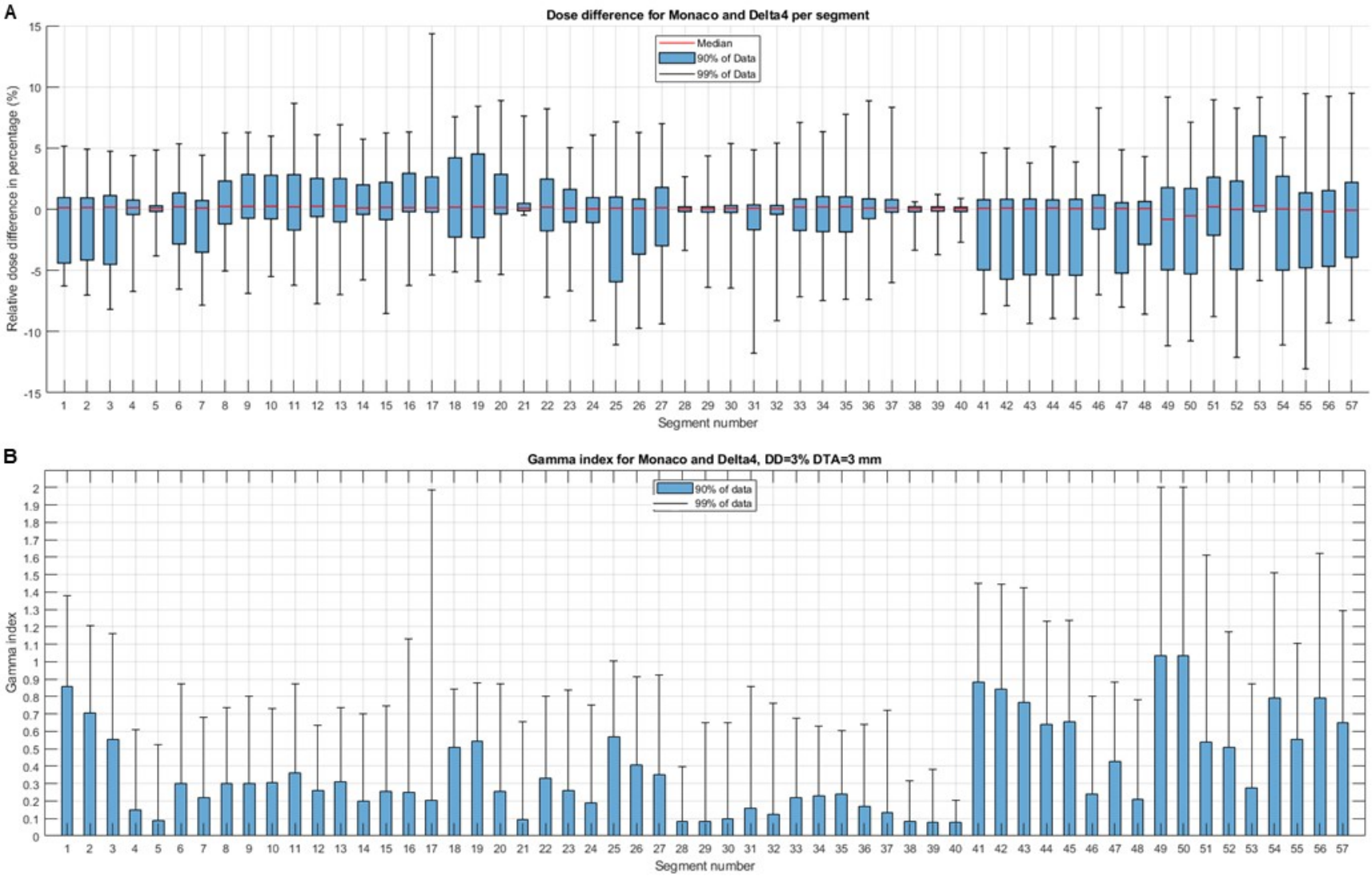

Figure 28 - Dose difference (A) and Gamma-index (B) for Monaco and Delta4 phantom with 1069 detectors per segment, including median (red line), 90% borders (blue line) and 99% borders (black line).

3.3.6 Logfile & Delta4 – per 200ms

This part compares the results of the Logfiles and Delta4 dose distribution at a timescale of 200ms. The dose distributions are calculated in a cumulative way as shown in figure 29. One point in the coronal plane is selected (figure 24A) and the buildup of dose over time is plotted in figure 24B-C.

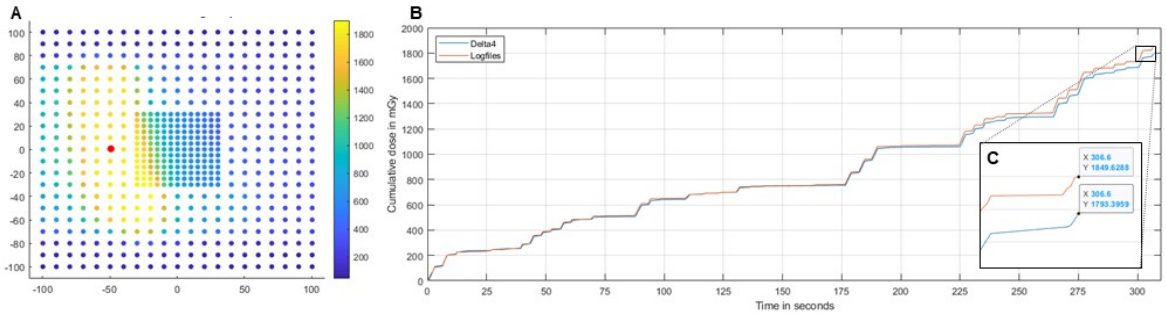

Figure 29 – One point in the coronal plane (A) with corresponding cumulative doses build-up (B) for Delta4 (blue line) and Logfiles (red line). Zoomed in image of last segment (C).

Visually, the cumulative dose in the selected point is the same for the Logfiles and Delta4. However, after 225s there is an discrepancy between the cumulative dose recorded by the Delta4 and calculated with the Logfiles. In the end, the cumulative values are respectively 1850 and 1793 mGy for Logfiles and Delta3. This results in an absolute difference of 57 mGy and a relative difference of 3%.

For the comparison of multiple detector points, only points with a cumulative dose at the end of the irradiation of more than 90%, see figure 30. The relative dose was normalized to 1899 mGy (=maximum). This resulted in a group of 58 detectors with a range of 1726 to 1899 mGy. For this group the absolute and relative dose difference was determined per 200ms.

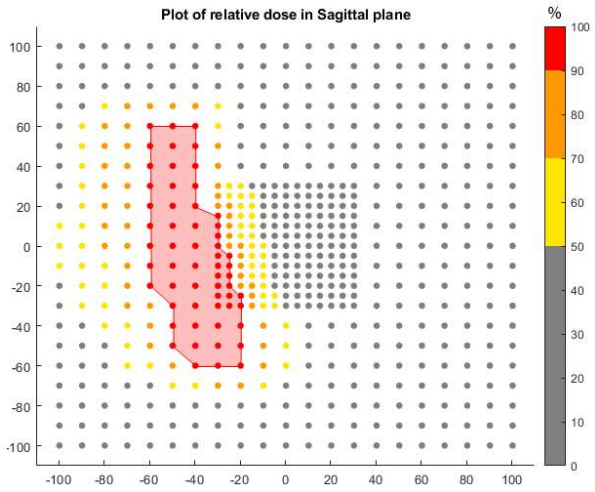

Figure 30 – Isodose distribution of sagittal Delta4 detector plane. 90% line includes 58 detector points (red area). Normalization is based on maximum cumulative dose.

The absolute dose difference has a range of -71 to 25 mGy for 58 selected detectors. A graphical representation of the data is shown in figure 31A, were the height of each bar represents the range of absolute DD for 58 selected detectors. On the x-axis all the 58 segments are labeled, whereas the bar width is 200ms. The empty space between the segments is the non-irradiation time period.
The relative dose difference has a range of -98.1 to 9.1% for the first 2 segments (=timespan of 8.4s), see figure 31B. Segments 3-7 have a DD of -4.0 to 7.1% (figure 31C), whereas the DD of the rest of the segments (after 33s) is between -5.2 and 5.3%.

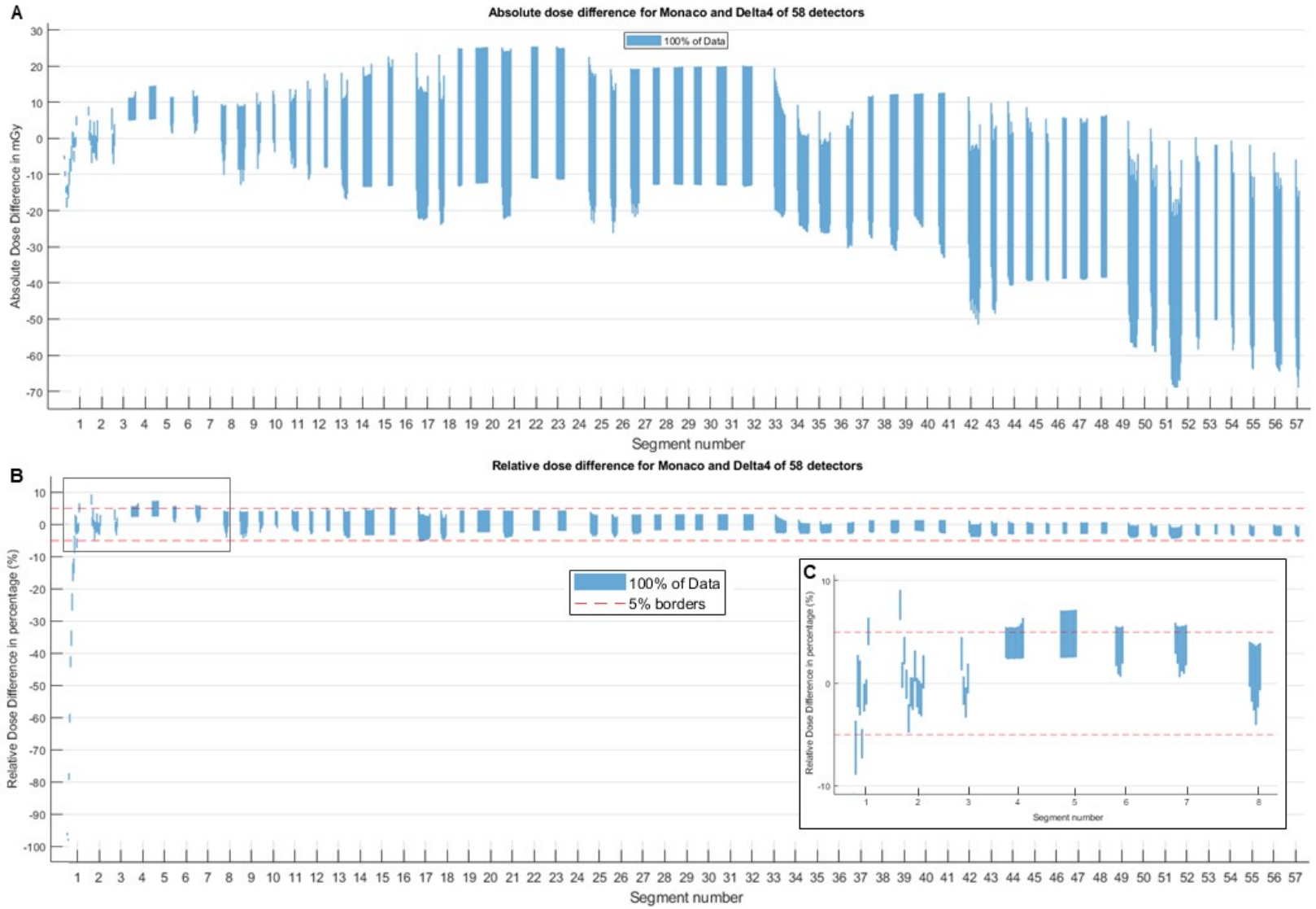

Figure 31 – Absolute(A) and relative (B,C) dose difference for Monaco and Delta4 of 58 detector points per 200 ms.

4. Discussion

In this thesis we have successfully implemented logfile dose reconstruction and demonstrated it's potential for use as a QA tool. The accuracy of the reconstructions are according to the current acceptable passing criteria for IMRT regarding the total RT-plan, per field and per segment. When reconstructing dose distributions on a timescale of 200ms, the accuracy is slightly lower. Further development of the software/workflow can improve the accuracy and can add new features.

4.1 Validation

In the first validation experiment, there was good correlation between the detectors values of the Delta4 in the Scandidos software and in the final DataObject. However, there was a slight difference between the two, that might have been caused by the processing steps in the software. Particularly in the last step when a 3D grid was created and interpolation was performed. Also the use of single-precision variables in Matlab might have caused an rounding error. In the end, the impact of this error is minimal when considering the final analysis.

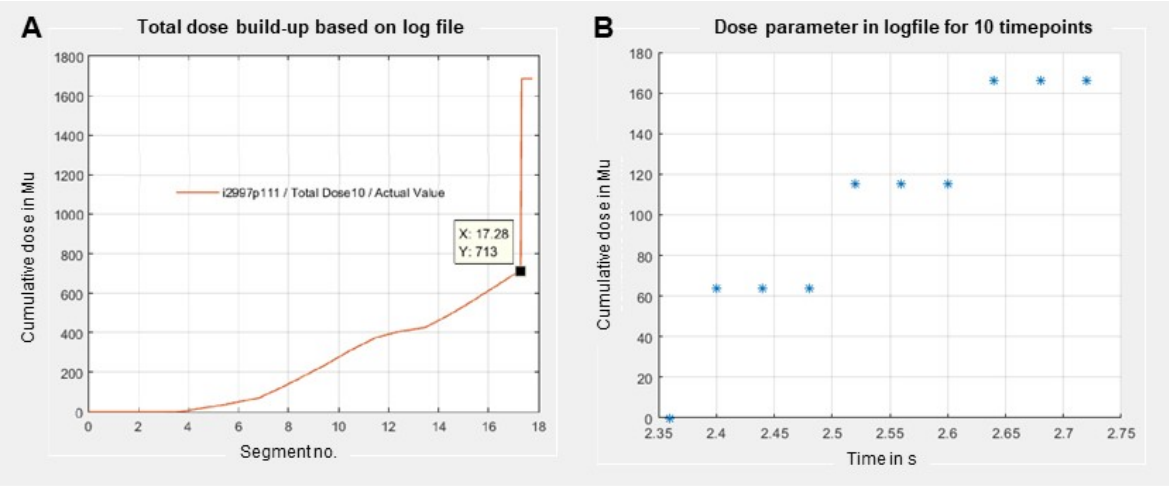

Figure 32 – Two examples of inconsistencies in the logfile. In first example (A), a false dose is reported at the end of the RT-plan, adopted from A.A. van Appeldoorn, UMC Utrecht. In the second example (B), there is a false representation of the cumulative dose, since it is flat for 3 timestamps while the dose rate is not zero.

In the logfile there were inconsistencies in the dose parameters. They did not share the same timestamp at the end of a segment. We performed a workaround, by choosing the dose parameter that had the best match with the Delta4, in terms of segment duration. However, this issue could be solved by using an extra device which only monitors if radiation is present. Another interesting point is the correctness of the dose parameters. Figure 32A shows an isolated case when a false dose is reported at the end of the RT-plan. In figure 32B, an erroneous value of the cumulative dose is displayed. This error might also cause ripples in the slope of figure 14, since GPUMCD uses the "Dose/Raw value" parameter for dose calculations. Fortunately, the latter issue has been solved with a recent machine software update. Both examples demonstrate the need for accuracy in the logfile, since an error may persist throughout the final dose distribution. Therefore, also quality assurance of the logfile should be performed.

The validation experiments were an important part in creating the software. Also in the future, these experiments play an important role, for example in case of further software development or after updates of the MR-LINAC and Delta4 phantom.

4.2 Time-synchronization

In our setup, execution of the RT-plan is performed on a step-and-shoot basis. This results in time periods of irradiation and non-irradiation, which can be used for identifying individual fields and segments. Therefore, time-synchronization is straight forward using a timescale of per beam or per segment. However, problems arise when a sub-segment timescale is required. The length of a irradiation segment, recorded by the Delta4, is not the same as dictated by the logfile. So, the start and end of a segment cannot be used for synchronization. One solution is to represent the dose values in a cumulative manner, so that the cumulative doses can be synchronized at the end of each segment. In this way, subsegment time-scales are possible. A drawback of this solution is, that no direct comparison of the two (delta4 and logfile) sub-segment pieces can be performed.
Another area of improvement is the sampling rate of the RAW data. Each consecutive machine state is saved in the logfile at an interval of 40ms (or 25 Hz). The sampling interval of the Delta4 is 25 ms (40 Hz). In our analysis we chose a time-scale of 200ms to limit the amount of data being generated, but also since it is a multiply of both sampling intervals. It would be more convenient if the sample interval of the Delta4 is 20ms. Synchronization of the two time-axis could (theoretically) be done more accurately. Another advance of a 20ms sample interval is the flexibility in the choice of time-scale, since sample intervals are multiply of each other. When the length of a consecutive datapackage is slightly different, strong aliasing effects may occur. However, the impact of an improved Delta4 sample interval for our current setup would be minimal, since we use the step-and-shoot approach of IMRT. For this method we can utilizes time intervals of non-irradiation for synchronization. However, Volumetric modulated arc therapy (VMAT) might benefit since this is a radiation therapy technique that delivers the radiation dose continuously as the treatment machine rotates. In this scenario, synchronization based on non-irradiation intervals cannot be performed and an adjusted Delta4 sample interval could help synchronize the two continuous time-axis.
Time-synchronization is important and can easily be performed on a segmental timescale when using IMRT, step-and-shoot. Adjustment of the Delta4 sample rate and short simple RT-plans may characterize both systems and improve synchronization on a sub-segment timescale. These recommendations may also help for synchronization of new continuous radiation therapy techniques. As a final recommendation, new structures should be added to the DataObject for saving the time-axis for convenience.

4.3 Analysis

In our analysis we compared different dose distributions, stored in DataObjects. Although the DataObject were well structured and helpful in the comparisons, minor improvements can increase the accuracy. For the Delta4 DataObject, we used nearest neighbor interpolation, since we did not want to create new values apart from the measured ones. This resulted in a pixelated dose distribution of the measured Delta4 values, but which cannot be registered to the logfile dose distribution. The use of back projection around the same rotation point can result in a more smooth distribution with the option for registration. Moreover these newly calculated values could also be used for evaluation in the analysis.

The voxel size of the Delta4 DataObject was 5x5x5 mm with dimensions of 43x43x43 voxels. These sizes were chosen, based on the minimal spacing between the diodes. Moreover, processing of the DataObject was fast because of the limited grid size. However, the actual diodes have an size of 1 mm in diameter and a height of 0.05 mm. Therefore, a voxel size of 1x1x1 mm would be more appropriate, resulting in an 215x215x215 grid. In this way, the Delta4 DataObject can directly be compared with the logfile DataObject. To limit the amount of data, a 2D grid can be used, resulting in two planes of 215x215 mm. Nonetheless, an additional transformation of the planes into an 3D grid is required for calculation of the gamma index.
We used common QA techniques in our comparison analysis, each with its own limitations. For example, visual inspection in different planes does not cover the total dataset, whereas the dose difference can be large in regions with a high dose gradient. Though the γ-index combines both DD and DTA into a single number, it's outcome is an abstract metric and cannot directly pinpoint the cause in case of a high γ-index. Therefore, multiple techniques are required to confirm good correspondence among dose distributions.
Here we successfully demonstrated that an MR-LINAC logfile can be used as a QA tool, but our results are based on a single fractional patient RT-plan. In order to gain experience with logfile based dose reconstruction, more results of different RT-plans are needed. Therefore integration into the current daily adaptive MRIgRT workflow is important, since in this setup patient RT-plans can easily be processed.

4.4 Integration of logfile QA

After implementation of the recommendations mentioned above, the next step is integration of logfile QA (see figure 33, yellow line) into the current daily adaptive MRIgRT workflow (see figure 33, blue line). First of all, the specific systems that provide the inputs for the logfile QA need to be identified and the data needs to be stored. Then, a script can semi-automatically process the data and generate a report. A dedicated PC will perform all these steps. In this setup, logfile QA has a passive role and experience is gained with logfile dose reconstruction. Also in this phase, optimization of the workflow can be done. When intrafractional adaptive MRIgRT is available (see figure 33, orange line), logfile QA will have a more active role. In this setup, logfile QA will test the updated RT plan and can interrupt the irradiation process if required. Keep in mind, that the results from logfile QA have a delay, since it takes time to process, compute and analyses the data. Therefore, the detection of errors in the updated RT-plan cannot be displayed real-time.
One of the big challenges is optimizing and reducing the processing time of the logfile QA workflow. Kontaxis et al. reported a calculation time of 8.5 min using logfile based dose reconstruction [29]. This did not include the time required for extraction of the logfile and collection of the Dicom data. The actual radiation delivery took on average 5.5 min on the MR-LINAC. His work shows that logfile based dose reconstruction can currently be applied for assessment of the delivered dose after treatment completion on a daily basis.

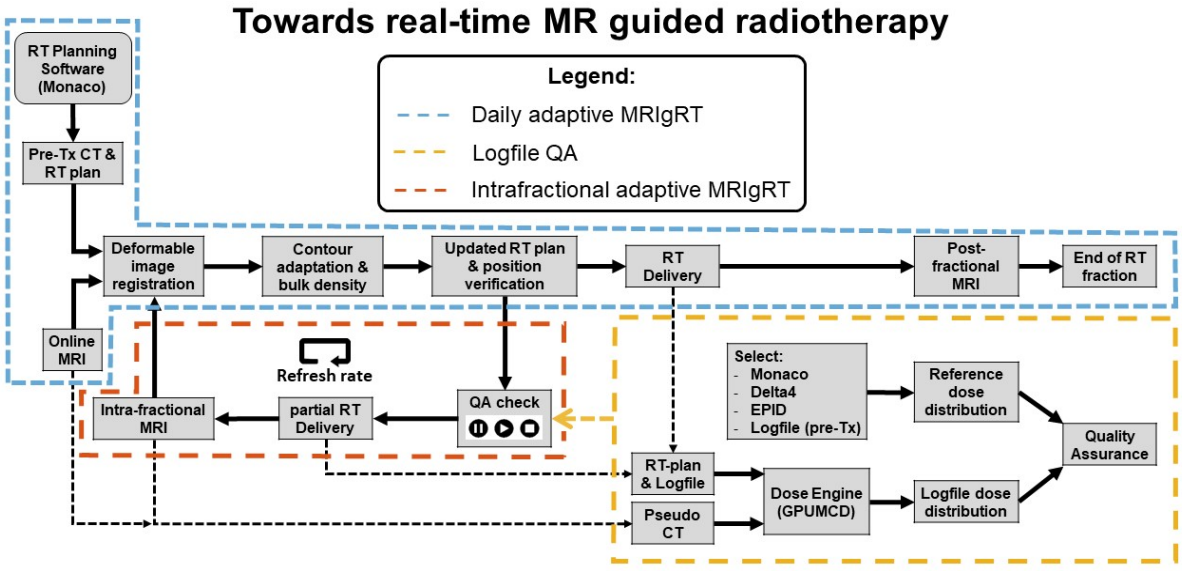

Figure 33 – Diagram of the current daily adaptive MRI guided radiotherapy (MRIgRT) workflow (dashed blue line). Future implementation of Logfile QA (dashed yellow line) and intrafractional adaptive MRIgRT (dashed orange line).

4.5 Clinical potential

When logfile based dose reconstruction is general accepted for the MR-LINAC, it can be used as an QA tool equivalent to e.g. film QA or plan QA with the Delta4. Then, the full potential of the MR-LINAC can safely be explored using new irradiation techniques, like intrafractional adaptive MRIgRT. When these new adaptive algorithms are safely implemented by using logfile QA, they can handle anatomical changes during the radiotherapy course as if no motion was present [30]. This results in better dose conformity to the planning target volume and lower normal tissue involvement, for example in patients with rectal cancer [31]. Also hypofractionated MRI-guided RT treatments may be performed, for example, in prostate cancer patients. Using a soft-tissue contrast based tracking algorithm, instead of 20 fractions of 3.1 Gy, a hypofractionated RT scheme of 5x7.25 Gy can be given [29]. This may lead to improvement of tumor control and a higher quality of life after RT. In general, also compliance to radiotherapy may increase by shorter treatment courses for patients [32].

5. Conclusion

In this thesis, we have demonstrated accurate logfile based dose reconstruction on a total RT-plan and per beam timescale. Smaller timescales have a slightly higher error, which requires improvements. The Delta4 phantom MR+ can be used for physical dose measurements on a small timescale and can help optimize logfile based dose reconstruction.

Appendices

A. Monaco vs Delta4

A.1 Total RT-plan

In this experiment we will compare the Monaco and the Delta4 dose distribution on a cumulative timescale. Only the voxels that correspond to the locations of the 1069 Delta4 detectors are used.

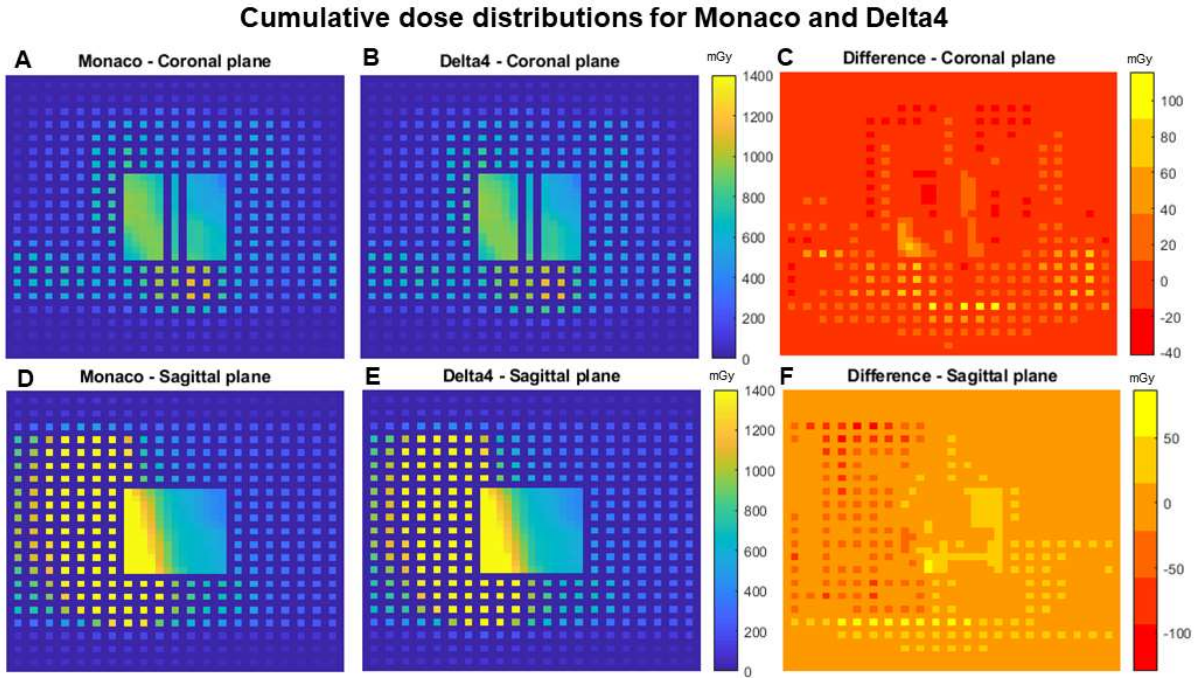

Appendix figure 1 - Cumulative dose distribution for Monaco (A & D) and Delta4 (B & E) with difference (C & F).

Appendix figure 1 shows the absolute dose measures per diode in the coronal and sagittal plane for the Monaco and Delta4. Maximal dose differences in the order of -40 to 100 mGy are observed in coronal plane. In the sagittal plane, maximum dose differences of around -100 up to 50 mGy are observed.

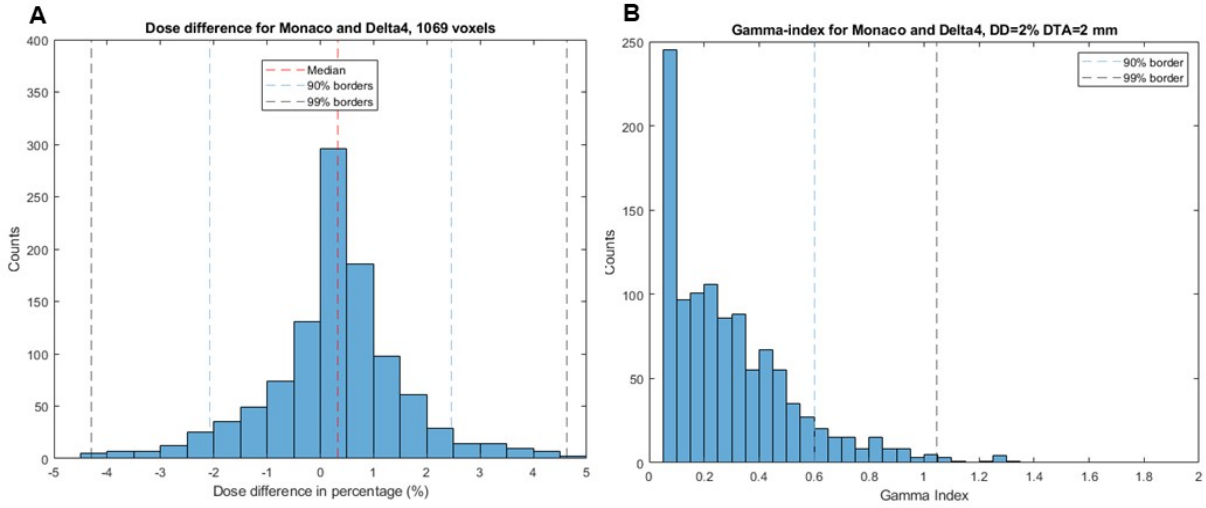

Appendix figure 2 – Dose difference (A) and Gamma-index (B) for Monaco and Delta4 phantom with 1069 detectors, including median (red line), 90% borders (blue lines) and 99% borders (black lines).

The dose difference between the Monaco and the for 1069 detectors of the Delta4 is plotted in figure 8A. A dose difference of -2.1 and 2.5% was found for 90% of the data and the range in dose difference was -4.3 and 4.6% for 99% of the data,. The gamma-index (DD=2% and DTA=2mm) is 0.60 and 1.05 for respectively 90% and 99% of the data (Appendix figure 2).

A.2 - Monaco vs Delta4, per beam

This section reports the results of the Monaco and Delta4 dose distribution per beam. Only 1069 voxels, related to the detector positions, are taken into account.

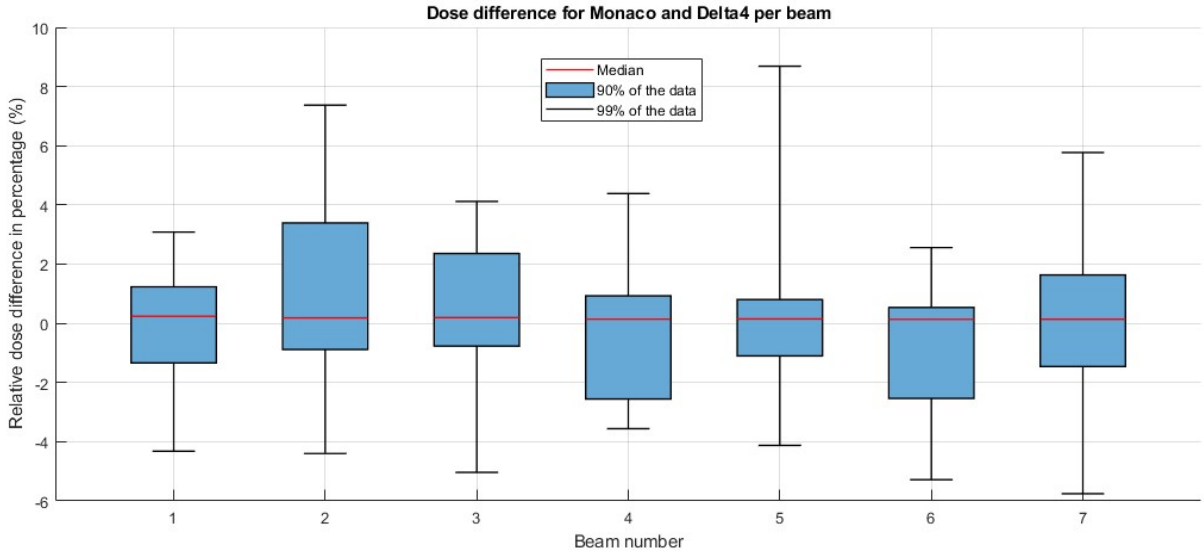

Appendix figure 3 – Dose Difference for Monaco and Delta4 per beam, including median (red line), 90% of the data (blue bar) and 99% of the data (whiskers).

The median dose difference is 0.15 to 0.24 % for all 7 beams (appendix figure 3). The relative DD for 90% of the data (= 962/1069 voxels) is -2.6 to 3.4% considering all beams. In 99% of the data (= 1058/1069 voxels), the DD is between -5.8 to 8.7%.

The gamma index for Monaco and Delta4 dose distributions is shown in figure 10. For the parameters, a DD of 5, 3 and 1% and a DTA of 5, 3 and 1 mm was chosen.
For DD=3% and DTA=3mm: In 90% of the data (=962/1069 voxels), a maximum gamma-index of 0.42 was observed, while 99% of the data (= 1058/1069voxels) a maximum gamma-index of 0.9 was noted.
For DD=2% and DTA=2mm: In 90% of the data (=962/1069 voxels), a maximum gamma-index of 0.63 was observed, while 99% of the data (= 1058/1069voxels) a maximum gamma-index of 1.4 was noted.
For DD=1% and DTA=1mm: In 90% of the data (= 962/1069 voxels), a maximum gamma-index of 1.26 was observed, while 99% of the data (= 1058/1069 voxels) a maximum gamma-index of 2.0 was noted.

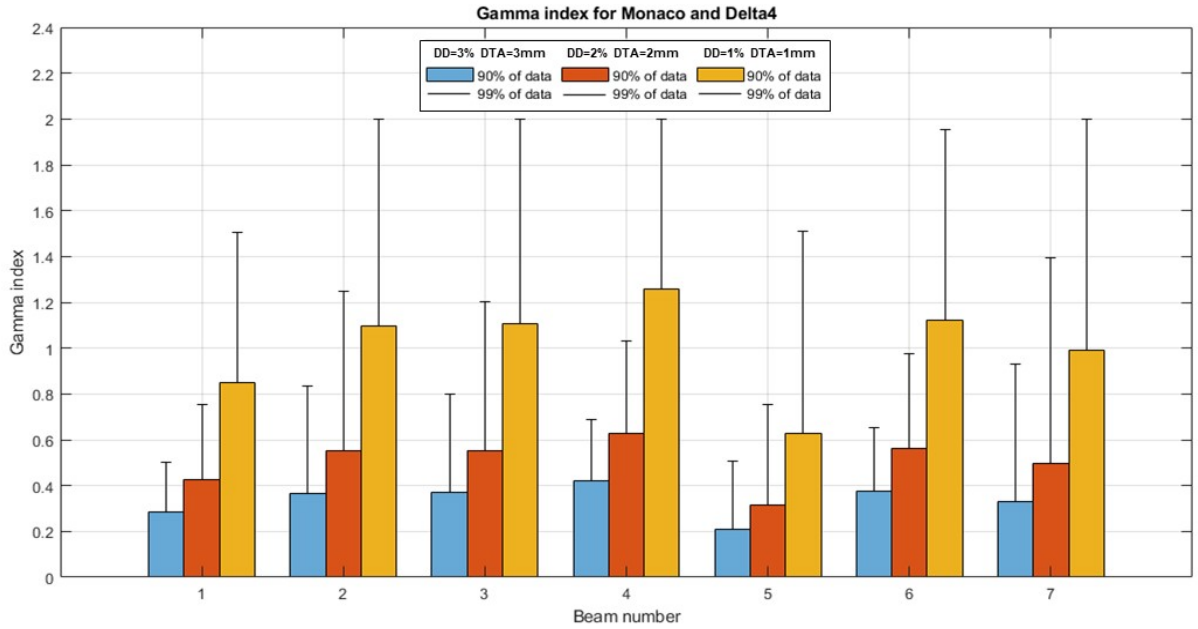

Appendix figure 4 – Gamma index for Monaco and Delta4 using DD of 3, 2 and 1% and a DTA of 3, 2 and 1 mm, displaying 90% of the data (blue bars) and 99% of the data (whiskers).

References

[1] A. van der Horst, A. C. Houweling, G. van Tienhoven, J. Visser, and A. Bel, 'Dosimetric effects of anatomical changes during fractionated photon radiation therapy in pancreatic cancer patients', *J. Appl. Clin. Med. Phys.*, vol. 18, no. 6, pp. 142–151, Oct. 2017, doi: 10.1002/acm2.12199.

[2] C. J. Moore *et al.*, 'Developments in and experience of kilovoltage X-ray cone beam image-guided radiotherapy', *Br. J. Radiol.*, vol. 79 Spec No 1, pp. S66-78, Sep. 2006, doi: 10.1259/bjr/68255935.

[3] I. J. Das, K. P. McGee, N. Tyagi, and H. Wang, 'Role and future of MRI in radiation oncology', *Br. J. Radiol.*, vol. 92, no. 1094, p. 20180505, Nov. 2018, doi: 10.1259/bjr.20180505.

[4] H. Chandarana, H. Wang, R. H. N. Tijssen, and I. J. Das, 'Emerging Role of MRI in Radiation Therapy', *J. Magn. Reson. Imaging JMRI*, vol. 48, no. 6, pp. 1468–1478, Dec. 2018, doi: 10.1002/jmri.26271.

[5] J. J. W. Lagendijk *et al.*, 'MRI/linac integration', *Radiother. Oncol. J. Eur. Soc. Ther. Radiol. Oncol.*, vol. 86, no. 1, pp. 25–29, Jan. 2008, doi: 10.1016/j.radonc.2007.10.034.

[6] B. W. Raaymakers *et al.*, 'Integrating a 1.5 T MRI scanner with a 6 MV accelerator: proof of concept', *Phys. Med. Biol.*, vol. 54, no. 12, pp. N229–N237, May 2009, doi: 10.1088/0031-9155/54/12/N01.

[7] A. Dunlop *et al.*, 'Daily adaptive radiotherapy for patients with prostate cancer using a high field MR-linac: Initial clinical experiences and assessment of delivered doses compared to a C-arm linac', *Clin. Transl. Radiat. Oncol.*, vol. 23, pp. 35–42, Jul. 2020, doi: 10.1016/j.ctro.2020.04.011.

[8] V. W. C. Wu, A. P. L. Ng, and E. K. W. Cheung, 'Intrafractional motion management in external beam radiotherapy', *J. X-Ray Sci. Technol.*, vol. 27, no. 6, pp. 1071–1086, 2019, doi: 10.3233/XST-180472.

[9] M. Miften *et al.*, 'Tolerance limits and methodologies for IMRT measurement-based verification QA: Recommendations of AAPM Task Group No. 218', *Med. Phys.*, vol. 45, no. 4, pp. e53–e83, Apr. 2018, doi: 10.1002/mp.12810.

[10] J. L. Bedford, Y. K. Lee, P. Wai, C. P. South, and A. P. Warrington, 'Evaluation of the Delta4 phantom for IMRT and VMAT verification', *Phys. Med. Biol.*, vol. 54, no. 9, pp. N167-176, May 2009, doi: 10.1088/0031-9155/54/9/N04.

[11] R. Sadagopan, J. A. Bencomo, R. L. Martin, G. Nilsson, T. Matzen, and P. A. Balter, 'Characterization and clinical evaluation of a novel IMRT quality assurance system', *J. Appl. Clin. Med. Phys.*, vol. 10, no. 2, pp. 104–119, May 2009, doi: 10.1120/jacmp.v10i2.2928.

[12] J. H. W. de Vries *et al.*, 'Characterization of a prototype MR-compatible Delta4 QA system in a 1.5 tesla MR-linac', *Phys. Med. Biol.*, vol. 63, no. 2, p. 02NT02, 11 2018, doi: 10.1088/1361-6560/aa9d26.

[13] B. A. Hargreaves, P. W. Worters, K. B. Pauly, J. M. Pauly, K. M. Koch, and G. E. Gold, 'Metal-Induced Artifacts in MRI', *Am. J. Roentgenol.*, vol. 197, no. 3, pp. 547–555, Sep. 2011, doi: 10.2214/AJR.11.7364.

[14] C. Legrand, '49. Current uses of log files in the radiotherapy quality assurance workflow for IMRT and VMAT techniques', *Phys. Med.*, vol. 44, p. 24, Dec. 2017, doi: 10.1016/j.ejmp.2017.10.074.

[15] N. Tyagi, K. Yang, D. Gersten, and D. Yan, 'A real time dose monitoring and dose reconstruction tool for patient specific VMAT QA and delivery', *Med. Phys.*, vol. 39, no. 12, pp. 7194–7204, Dec. 2012, doi: 10.1118/1.4764482.

[16] J. Qian *et al.*, 'Dose reconstruction for volumetric modulated arc therapy (VMAT) using cone-beam CT and dynamic log files', *Phys. Med. Biol.*, vol. 55, no. 13, pp. 3597–3610, Jul. 2010, doi: 10.1088/0031-9155/55/13/002.

[17] M. J. Menten *et al.*, 'Automatic reconstruction of the delivered dose of the day using MR-linac treatment log files and online MR imaging', *Radiother. Oncol.*, vol. 145, pp. 88–94, Apr. 2020, doi: 10.1016/j.radonc.2019.12.010.

[18] C. Kontaxis, G. H. Bol, J. J. W. Lagendijk, and B. W. Raaymakers, 'DeepDose: towards a fast dose calculation engine for radiation therapy using deep learning', *Phys. Med. Biol.*, Feb. 2020, doi: 10.1088/1361-6560/ab7630.
[19] Nederlandse Commissie voor Stralingsdosimetrie, 'NCS-18: Code of Practice for the Absorbed Dose Determination in High Energy Photon and Electron Beams', Aug. 2012.
[20] S. Hissoiny, A. J. E. Raaijmakers, B. Ozell, P. Després, and B. W. Raaymakers, 'Fast dose calculation in magnetic fields withGPUMCD', *Phys. Med. Biol.*, vol. 56, no. 16, pp. 5119–5129, Jul. 2011, doi: 10.1088/0031-9155/56/16/003.
[21] M. Clements, N. Schupp, M. Tattersall, A. Brown, and R. Larson, 'Monaco treatment planning system tools and optimization processes', *Med. Dosim.*, vol. 43, no. 2, pp. 106–117, Jun. 2018, doi: 10.1016/j.meddos.2018.02.005.
[22] V. Feygelman, K. Forster, D. Opp, and G. Nilsson, 'Evaluation of a biplanar diode array dosimeter for quality assurance of step-and-shoot IMRT', *J. Appl. Clin. Med. Phys.*, vol. 10, no. 4, pp. 64–78, Sep. 2009, doi: 10.1120/jacmp.v10i4.3080.
[23] I. J. Yeo and J. O. Kim, *A Procedural Guide to Film Dosimetry with Emphasis on IMRT*. Medical Physics Publishing Corporation, 2004.
[24] D. A. Low, W. B. Harms, S. Mutic, and J. A. Purdy, 'A technique for the quantitative evaluation of dose distributions', *Med. Phys.*, vol. 25, no. 5, pp. 656–661, 1998, doi: https://doi.org/10.1118/1.598248.
[25] M. Geurts, *CalcGamma*. 2018.
[26] S. Hariri Tabrizi, N. Heidarloo, and M. Tavallaie, 'Introduction of a Reliable Software for the Calculation of the Gamma Index', *Iran. J. Med. Phys.*, vol. 17, no. 3, pp. 133–136, 2020, doi: 10.22038/ijmp.2019.39178.1557.
[27] D. A. Low, J. M. Moran, J. F. Dempsey, L. Dong, and M. Oldham, 'Dosimetry tools and techniques for IMRT', *Med. Phys.*, vol. 38, no. 3, pp. 1313–1338, Mar. 2011, doi: 10.1118/1.3514120.
[28] G. A. Ezzell *et al.*, 'IMRT commissioning: multiple institution planning and dosimetry comparisons, a report from AAPM Task Group 119', *Med. Phys.*, vol. 36, no. 11, pp. 5359–5373, Nov. 2009, doi: 10.1118/1.3238104.
[29] C. Kontaxis *et al.*, 'Delivered dose quantification in prostate radiotherapy using online 3D cine imaging and treatment log files on a combined 1.5T magnetic resonance imaging and linear accelerator system', *Phys. Imaging Radiat. Oncol.*, vol. 15, pp. 23–29, Jul. 2020, doi: 10.1016/j.phro.2020.06.005.
[30] D. Winkel *et al.*, 'Adaptive radiotherapy: The Elekta Unity MR-linac concept', *Clin. Transl. Radiat. Oncol.*, vol. 18, Apr. 2019, doi: 10.1016/j.ctro.2019.04.001.
[31] M. P. W. Intven *et al.*, 'Online adaptive MR-guided radiotherapy for rectal cancer; feasibility of the workflow on a 1.5T MR-linac: clinical implementation and initial experience', *Radiother. Oncol.*, vol. 154, pp. 172–178, Jan. 2021, doi: 10.1016/j.radonc.2020.09.024.
[32] S. Chin *et al.*, 'Magnetic resonance-guided radiation therapy: A review', *J. Med. Imaging Radiat. Oncol.*, vol. 64, no. 1, pp. 163–177, Feb. 2020, doi: 10.1111/1754-9485.12968.